

# Learning Decentralized Swarms Using Rotation Equivariant Graph Neural Networks

Taos Transue · Bao Wang

Received: date / Accepted: date

**Abstract** The orchestration of agents to optimize a collective objective without centralized control is challenging yet crucial for applications such as controlling autonomous fleets, and surveillance and reconnaissance using sensor networks. Decentralized controller design has been inspired by self-organization found in nature, with a prominent source of inspiration being flocking; however, decentralized controllers struggle to maintain flock cohesion. The graph neural network (GNN) architecture has emerged as an indispensable machine learning tool for developing decentralized controllers capable of maintaining flock cohesion, but they fail to exploit the symmetries present in flocking dynamics, hindering their generalizability. We enforce rotation equivariance and translation invariance symmetries in decentralized flocking GNN controllers and achieve comparable flocking control with 70% less training data and 75% fewer trainable weights than existing GNN controllers without these symmetries enforced. We also show that our symmetry-aware controller generalizes better than existing GNN controllers. Code and animations are available at [github.com/Utah-Math-Data-Science/Equivariant-Decentralized-Controllers](https://github.com/Utah-Math-Data-Science/Equivariant-Decentralized-Controllers).

**Keywords** machine learning · graph neural networks · flocking · equivariance · computational learning theory

**Mathematics Subject Classification (2020)** MSC 68T05 · MSC 68Q32 · MSC 68T42

---

Taos Transue · Bao Wang  
Department of Mathematics, University of Utah, 155 South 1400 East, Salt Lake City, Utah 84112, USA.

Bao Wang  
Scientific Computing and Imaging Institute, University of Utah, 72 S Central Campus Drive, Salt Lake City, Utah 84112, USA.  
Corresponding author E-mail: [taos.j.transue@gmail.com](mailto:taos.j.transue@gmail.com)  
E-mail: [wangbaonj@gmail.com](mailto:wangbaonj@gmail.com)

## 1 Introduction

Orchestrating a system of agents to optimize a collective objective is crucial in autonomous vehicle control [28], surveillance and reconnaissance with sensor networks [1], and beyond [17]. Designing controllers for these systems is often inspired by self-organization in nature. A prominent source of inspiration is flocking: myxobacteria travel in clusters to increase the concentration of an enzyme they use to stun their prey, making predation more effective for each individual [5]; pelicans follow a leader pelican in a vee formation, taking advantage of special aerodynamics to reduce the energy expenditure of flight [40]; and schools of fish coordinate their movement in several formations, minimizing each individual’s risk of predation [27].

When designing a controller to optimize a collective objective, there are three pertinent questions: (1) What objective should an agent optimize individually? (2) What information about other agents or the environment does an agent need to act? (3) How do the actions of each agent culminate in optimizing the collective objective? The first two questions were studied for flocking controllers in [30], where Reynolds sought to reproduce bird flocking and created one of the earliest simulations of flock-like motion. His simulation had each agent (so-called “bird-oid” or “boid”) balance the following three objectives:

- **Alignment:** Each agent should steer toward its neighbors’ average direction.
- **Cohesion:** Each agent should move toward the average position of its neighbors.
- **Separation:** Each agent should move away from its neighbors if they are too close.

To optimize these objectives, each agent used the position and velocity of all other agents. With qualitative answers to questions (1) and (2), Reynolds programmed agents that “participate in an acceptable approximation of flock-like motion.” Since flock-like motion was not yet quantified, question (3) remained unanswered. Later, researchers quantified flock-like motion with *asymptotic flocking* and *separation* (Definitions 1 and 2). Now, question (3) is answered by arguing that a given controller induces asymptotic flocking.

Notable flocking controllers include those designed in [35, 12]. In [35], Tanner et al. set the agents’ accelerations equal to a term that encourages alignment plus the negative gradient of a potential function for cohesion and separation. If the graph representing what agents can exchange information is fully connected, asymptotic flocking and separation are guaranteed. In [12], Cucker and Smale define the agents’ accelerations in a way that aligns their velocities while preserving the momentum of the flock. They achieve this with an “influence function,” which gauges an agent’s influence on another as a function of their distance. The benefit of momentum conservation is that the limiting velocity of the flock can be computed from the flock’s initial conditions. Cucker and Smale’s controller guarantees asymptotic flocking, and guarantees

separation with singular influence functions [11,22]. Further developments in flocking controllers can be viewed as adding constraints when optimizing a collective flocking objective. Developments that add constraints to Tanner et al.'s controller include leader following – requiring the flock to follow a leader agent [15], and segregation – flocking while having agents cluster into preassigned groups [32]. Developments that add constraints to the Cucker-Smale controller include encouraging the agents to be a fixed distance  $R > 0$  from each other using a PID controller [26], and pattern formation via control terms added to the agents' acceleration [24,8,9].

All these controllers require agents to exchange information with all others agents, making them **centralized controllers**. As the number of agents grows, an increasingly prominent alternative is **decentralized controllers** where agent communication is represented by a sparse graph. In a flock of  $N$  agents, a centralized controller requires each agent to communicate with  $N - 1$  agents, resulting in quadratic ( $\mathcal{O}(N^2)$ ) communication overhead growth. Moreover, a centralized controller imposes a bound on  $N$  when separation is required, and each agent has a maximum communication distance. Maximum communication distance constraints arise in wireless communications where the power required to send information over a distance  $r$  is proportional to  $r^p$  for some  $p \in [2, 4)$  [1]. A maximum communication distance  $R_{\text{comm}}$  and a minimum separation of  $R_{\text{min}}$  bound  $N$  because only a finite number of disjoint balls with diameter  $2R_{\text{min}}$  can be packed into a ball whose diameter is the maximum diameter of the flock ( $2R_{\text{comm}}$ ). **Decentralization is crucial for building scalable flocking controllers**, but compared to centralization, decentralization requires additional assumptions to guarantee asymptotic flocking and may not be compatible with other guarantees (e.g., separation).

Examples of decentralized controllers include those proposed by Tanner et al. [35,36]. The controller proposed in [35] uses a fixed connected communication graph to guarantee asymptotic flocking,<sup>1</sup> but it does not guarantee separation because nonadjacent agents cannot communicate. Though flock cohesion is guaranteed, adjacent agents may need to communicate over arbitrarily large distances while the controller is active. Instead of a fixed agent neighborhood, the neighborhood of an agent in [36] changes over time by only containing other agents currently within the agent's communication radius  $R_{\text{comm}}$ . In this case, the authors guarantee asymptotic flocking and separation assuming that the communication graph is connected for all time; Fig. 1 shows that this assumption is invalid for some initial conditions. In [15], the authors propose a decentralized flocking controller with time-dependent agent neighbors and a leader following constraint, but they only test the controller with a fully connected communication graph. Without a fixed communication graph, decentralized flocking controllers struggle to maintain communication graph connectivity and flock cohesion – a requirement for effectively optimizing the collective objective.

---

<sup>1</sup> In practice, the communication graph can be constructed using the idea of virtual nodes; see e.g., [34,16].

As suggested by question (2), a plausible approach to improve decentralized controllers is providing more information to each agent. All the controllers we described, centralized or decentralized, only use information from the current time. Tolstaya et al. [37] apply machine learning (ML) to leverage current and past information. Fig. 1 shows that their ML controller can achieve asymptotic flocking for flock initial conditions where the controller in [36] fails (see Fig. 1). The ML controller works by having each agent retain a summary of the information it receives during the current time step and, during the next time step, send that summary to its neighbors. In addition, each agent retains a summary of the summaries it receives to send to its neighbors later, and this recursion continues up to  $K - 1$  time steps in the past. This process gives each agent access to information  $K$  hops away in the communication graph. In training, the ML controller learns to utilize patterns in how the information exchanged in the network changes over time. Though Tolstaya et al. [37] have found a way to provide additional information to each agent, their ML controller processes the information suboptimally. The flocking controllers in [35, 12] exhibit crucial symmetries, e.g., rotation equivariance, that have been ignored. Symmetry-aware ML models have demonstrated remarkable advantages in physical congruence and data efficiency [10, 13, 38, 2]. We aim to bridge this gap in this paper.

## 2 Our contributions

We improve decentralized ML flocking controllers by enforcing rotation equivariance into time-delayed aggregation GNNs (TDAGNNs) [37], restoring the symmetries of non-ML flocking controllers. We summarize our key contributions as follows:

- We present a simple yet efficient rotation equivariant convolutional neural network (CNN) and integrate it into TDAGNN for learning decentralized flocking.
- We justify the theoretical advantages of rotation equivariance in learning decentralized flocking by demonstrating better generalization compared to non-equivariant controllers.
- We demonstrate the advantages of our new ML controller in decentralized flocking, leader following, and obstacle avoidance.

### 2.1 Organization

We organize this paper as follows. In section 3, we review some related works on flocking controllers. In section 4, we present our rotation equivariant GNN for decentralized flocking. In section 5 and section 6, we analyze the generalization advantages of the rotation equivariant GNN for learning decentralized flocking and verify its effectiveness. Technical proofs and additional details are provided in the appendix.

### 3 Background

#### 3.1 Flock representation and definitions

Let  $\mathbf{X} = [\mathbf{x}_1, \dots, \mathbf{x}_N] \in \mathbb{R}^{2 \times N}$  be the position vectors of  $N$  agents,  $\dot{\mathbf{X}}$  be their velocities, and  $\mathbf{r}_{ij} = \mathbf{x}_i - \mathbf{x}_j$  be the relative position. We formulate the alignment and cohesion rules for asymptotic flocking as follows:

**Definition 1 (Asymptotic flocking [7])** A flock of  $N$  agents flocks asymptotically if and only if the following two conditions are satisfied: (1) **Alignment**:  $\lim_{t \rightarrow \infty} \max_{i,j} \|\dot{\mathbf{r}}_{ij}(t)\| = 0$ , and (2) **Cohesion**:  $\sup_{0 \leq t < \infty, i,j} \|\mathbf{r}_{ij}(t)\| < \infty$ .

Asymptotic flocking is usually the primary objective of flocking controllers. Controllers can also make guarantees concerning how their objectives are met, such as agent separation, which is defined as follows:

**Definition 2 (Agent  $R_{\min}$ -separation)** Let  $R_{\min} \geq 0$ . Agents are separated if for all time  $t$ ,  $\|\mathbf{r}_{ij}(t)\| \geq R_{\min}$ .

Other objectives or guarantees beyond those mentioned include segregation [32], where agents cluster into preassigned groups, and pattern formation [24, 8, 9].

The acceleration of the  $i$ -th agent is  $\ddot{\mathbf{x}}_i = \mathbf{a}_i(\mathbf{X}(t), \dot{\mathbf{X}}(t))$  where  $\mathbf{a}_i$  is the flocking controller. The design of  $\mathbf{a}_i$  ensures the flocking controller's objectives are met while maintaining its guarantees. The two main classes of flocking controllers – centralized and decentralized – are separated by whether they use the entire flock state  $(\mathbf{X}, \dot{\mathbf{X}})$  or only a subset of the columns of  $\mathbf{X}$  and  $\dot{\mathbf{X}}$  based on what agents can communicate.

#### 3.2 Centralized flocking

We recap on the centralized flocking controller from [35], which defines an agent's acceleration as

$$\ddot{\mathbf{x}}_i = \mathbf{a}_i(\mathbf{X}, \dot{\mathbf{X}}) := - \sum_{j=1}^N \dot{\mathbf{r}}_{ij} - \sum_{j=1}^N \nabla U(\|\mathbf{r}_{ij}\|), \quad (1)$$

where  $U : (0, \infty) \rightarrow \mathbb{R}$  is a potential function such that  $\lim_{r \rightarrow \infty} U(r) = \infty$  and  $r_* > 0$  is  $U$ 's unique minimizer representing the desired distance between two agents. The first summation aligns the agents' velocities, and the second summation uses  $U$  to control flock cohesion and agent separation. The potential function for  $U$  used in [36] is  $U(r) = 1/r^2 + \ln(r^2)$ , which encourages agents to be a distance  $r_* = 1$  from each other for cohesion and is singular at  $r = 0$  for separation. The function  $U$  can be changed to induce a variety of flock behaviors. For example, organizing leader-following [15] and segregating the agents into clusters [32].

### 3.3 Decentralized flocking

We briefly review the decentralized flocking controllers from [35,36]. The first decentralized controller [35] operates on a fixed sparse communication graph and defines an agent's acceleration as

$$\ddot{\mathbf{x}}_i = \mathbf{a}_i(\mathbf{X}, \dot{\mathbf{X}}) := - \sum_{j \in \mathcal{N}_i} \dot{\mathbf{r}}_{ij} - \sum_{j \in \mathcal{N}_i} \nabla U(\|\mathbf{r}_{ij}\|),$$

where  $\mathcal{N}_i$  is the neighborhood of agent  $i$ . This controller guarantees asymptotic flocking but does not guarantee separation because nonadjacent agents cannot communicate to avoid collision. Another drawback of this controller is that any adjacent agents must be able to communicate regardless of their spatial distance.

The second decentralized controller [36] defines the neighborhood of an agent to only include agents within radius  $R_{\text{comm}}$ , i.e.,  $\mathcal{N}_i(t) = \{j : j \neq i, \|\mathbf{r}_{ij}\| \leq R_{\text{comm}}\}$ . The agent's acceleration is defined as

$$\ddot{\mathbf{x}}_i = \mathbf{a}_i(\mathbf{X}, \dot{\mathbf{X}}) := - \sum_{j \in \mathcal{N}_i(t)} \dot{\mathbf{r}}_{ij} - \sum_{j \in \mathcal{N}_i(t)} \nabla U(\|\mathbf{r}_{ij}\|).$$

This controller guarantees asymptotic flocking and separation. However, it assumes the communication graph is connected for all time, but Fig. 1(a,b,c) show that this assumption may be invalid.

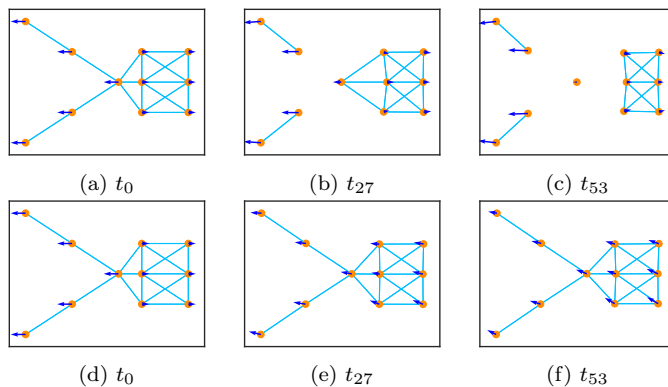


Fig. 1: Snapshots at times  $t_n$  of a flock of agents (orange dots) with velocities (blue arrows) and the flock's communication graph (light blue edges). When controlled by the time-dependent neighborhood decentralized flocking controller from Tanner et al. [36] (top row), the communication graph loses connectivity from time  $t_{27}$  onward. In contrast, the ML-based decentralized flocking controller from Tolstaya et al. [37] (bottom row), not trained on these agent initial conditions, successfully maintains communication graph connectivity and achieves asymptotic flocking.

### 3.4 ML-based decentralized flocking

#### 3.4.1 Time-delayed aggregation graph neural networks

We review TDAGNN from [37]. Let  $\mathcal{N}_i(t) = \{j : j \neq i, \|\mathbf{r}_{ij}\| \leq R_{\text{comm}}\}$  be the neighborhood of agent  $i$  at time  $t$ . Define a function  $\psi : \mathbb{R}^2 \times \mathbb{R}^2 \rightarrow \mathbb{R}^{C_1}$  and the recurrence relation at time  $t_n$  as

$$\mathbf{h}_i^1(t_n) = \sum_{j \in \mathcal{N}_i(t_n)} \psi(\mathbf{r}_{ij}(t_n), \dot{\mathbf{r}}_{ij}(t_n)), \quad (2)$$

$$\mathbf{h}_i^k(t_n) = \frac{1}{|\mathcal{N}_i(t_n)|} \sum_{j \in \mathcal{N}_i(t_n)} \mathbf{h}_j^{k-1}(t_{n-1}). \quad (3)$$

With  $\psi(\mathbf{r}_{ij}(t_n), \dot{\mathbf{r}}_{ij}(t_n))$  representing the message from agent  $j$  to agent  $i$  at time  $t_n$ ,  $\mathbf{h}_i^1(t_n)$  summarizes the messages within a one-hop neighborhood of agent  $i$ , and  $\mathbf{h}_i^2(t_n)$  summarizes the one-hop summaries from the previous time step within a one-hop neighborhood. Let  $\mathbf{H}_i(t_n) = [\mathbf{h}_i^1(t_n), \dots, \mathbf{h}_i^K(t_n)]$ . Finally, TDAGNN outputs the vector  $\phi(\mathbf{H}_i(t_n))$  for agent  $i$ 's acceleration, where  $\phi : \mathbb{R}^{C_1 \times K} \rightarrow \mathbb{R}^{C_{L_\phi+1}}$  is a 1D CNN with element-wise tanh activation after each convolutional layer except the last layer  $L_\phi$ . For agents in  $\mathbb{R}^2$ ,  $C_{L_\phi+1} = 2$ .  $K$  is the depth that the recurrence is computed to, and the larger  $K$  is, the more message summaries each agent needs to store; i.e., each agent  $i$  stores  $\mathbf{H}_i(t_{n-1})$  to be passed on at time  $t_n$ .

TDAGNN is trained using imitation learning (IL) reviewed in section 3.4.2. In our context of flocking control, the expert controller for IL is the centralized controller in Eqn. (1) with the potential function

$$U(r) = \begin{cases} 1/r^2 + \ln(r^2) & r \leq R_{\text{comm}}, \\ U(R_{\text{comm}}) & \text{else.} \end{cases} \quad (4)$$

The output of the expert controller  $\mathbf{a}_i$  is clamped so that  $\|\mathbf{a}_i(\mathbf{X}, \dot{\mathbf{X}})\|_\infty \leq 100$ . In [37],  $\psi : \mathbb{R}^2 \times \mathbb{R}^2 \rightarrow \mathbb{R}^6$  computes the terms that enter linearly into the centralized controller's acceleration:

$$\psi(\mathbf{r}_{ij}, \dot{\mathbf{r}}_{ij}) = [\dot{\mathbf{r}}_{ij}^\top, \|\mathbf{r}_{ij}\|^{-4} \mathbf{r}_{ij}^\top, \|\mathbf{r}_{ij}\|^{-2} \mathbf{r}_{ij}^\top]^\top. \quad (5)$$

TDAGNN trained using this  $U$  and  $\psi$  learns flocking control. Using the  $U$  from [32] and the  $\psi$  from [25], TDAGNN learns flocking control with segregation.

#### 3.4.2 Imitation learning

Flocking controllers are evaluated by whether they achieve their collective objective and by what intermediate steps they take to do so. For example, controllers that guarantee separation are devalued if they take intermediate steps that cause agent collisions. While non-ML controllers can be designed with these evaluation criteria in mind, ML controllers must be trained to

comply with the constraints imposed by these criteria. IL is a framework that trains ML controllers to produce the same output as a compliant “expert” controller. Let  $\mathbf{a}_i$  be the expert controller in Eqn. (4) and  $\phi$  be TDAGNN – a pupil controller. The IL loss function used in [37] is

$$\mathcal{L}(\mathbf{X}, \dot{\mathbf{X}}, \{\mathbf{H}_i\}_{i=1}^N) = \frac{1}{N} \sum_{i=1}^N \ell(\mathbf{a}_i(\mathbf{X}, \dot{\mathbf{X}}), \phi(\mathbf{H}_i)), \quad (6)$$

where  $\ell$  is another loss function (e.g., the squared error loss), and  $\mathbf{H}_i$  is the input to TDAGNN for agent  $i$ . Ideally, we would compute  $\mathcal{L}$  for every tuple  $(\mathbf{X}, \dot{\mathbf{X}}, \{\mathbf{H}_i\}_{i=1}^N)$  but this is intractable. Instead, we sample a training set from the space of these tuples using Dataset Aggregation (DAgger) reinforcement learning [31]. DAgger is employed in [37] to train TDAGNN as follows: Let  $E$  and  $T$  be the number of training epochs and time steps in a flocking simulation, respectively. At the beginning of each epoch  $e \in \{0, \dots, E - 1\}$ , an initial flock state  $(\mathbf{X}(t_0), \dot{\mathbf{X}}(t_0))$  is chosen from a dataset of initial conditions. Next, flocking is simulated for  $T$  time steps. For each  $n \in \{0, \dots, T - 1\}$ ,  $\mathbf{a}_i(\mathbf{X}(t_n), \dot{\mathbf{X}}(t_n))$  and  $\mathbf{H}_i(t_n)$  are computed. With probability  $\beta_e$ , the acceleration  $\mathbf{a}_i(\mathbf{X}(t_n), \dot{\mathbf{X}}(t_n))$  is used to update the flock state, computing  $\mathbf{X}(t_{n+1})$  and  $\dot{\mathbf{X}}(t_{n+1})$ ; otherwise, the acceleration  $\phi(\mathbf{H}_i(t_n))$  is used. Finally, the tuple  $(\mathbf{X}(t_n), \dot{\mathbf{X}}(t_n), \{\mathbf{H}_i(t_n)\}_{i=1}^N)$  is added to the training set. Once  $T$  time steps of flocking are complete, a batch  $\mathcal{B}$  of tuples is uniformly randomly sampled from the training set. The average value of  $\mathcal{L}$  over the batch is computed and TDAGNN’s weights are updated. We can update the weights more than once per epoch by sampling more batches.

### 3.5 Rotation equivariance and translation invariance of flocking controllers

Symmetry is a fundamental inductive bias for designing reliable and efficient neural networks [19, 20, 29, 41, 38]. The symmetry of a function  $f : X \rightarrow Y$  is often described by equivariance:  $f$  is equivariant if  $f(T_g(x)) = T'_g(f(x))$ , where  $T_g, T'_g$  are transformations representing the group element  $g$  on  $X$  and  $Y$ , respectively. If  $T'_g$  is the identity,  $f$  is invariant. A crucial property of GNNs is that their node feature aggregations are permutation invariant [14], and GNNs have also been extended to be roto-translation equivariant [33, 4]. For flocking, prominent controllers  $\mathbf{a}_i$  (e.g., [35, 12]) have the following symmetries:



- **Translation invariance:** For any  $\mathbf{t}_1, \mathbf{t}_2 \in \mathbb{R}^2$ , considering the controller in Eqn. (1), we have

$$\begin{aligned}
& \mathbf{a}_i(\mathbf{X} + \mathbf{t}_1 \mathbf{1}_N^\top, \dot{\mathbf{X}} + \mathbf{t}_2 \mathbf{1}_N^\top) \\
&= - \sum_{j=1}^N (\dot{\mathbf{x}}_i + \mathbf{t}_2) - (\dot{\mathbf{x}}_j + \mathbf{t}_2) - \sum_{j=1}^N \nabla U(\|\mathbf{x}_i + \mathbf{t}_1 - (\mathbf{x}_j + \mathbf{t}_1)\|) \\
&= - \sum_{j=1}^N \dot{\mathbf{r}}_{ij} - \sum_{j=1}^N \nabla U(\|\mathbf{r}_{ij}\|) \\
&= \mathbf{a}_i(\mathbf{X}, \dot{\mathbf{X}})
\end{aligned}$$

- **Rotation and reflection equivariance:** For any orthogonal matrix  $\mathbf{Q} \in \text{O}(2)$ , we have

$$\begin{aligned}
\mathbf{a}_i(\mathbf{Q}\mathbf{X}, \mathbf{Q}\dot{\mathbf{X}}) &= - \sum_{j=1}^N \mathbf{Q}\dot{\mathbf{x}}_i - \mathbf{Q}\dot{\mathbf{x}}_j - \sum_{j=1}^N \nabla U(\|\mathbf{Q}\mathbf{x}_i - \mathbf{Q}\mathbf{x}_j\|) \\
&= - \sum_{j=1}^N \mathbf{Q}\dot{\mathbf{r}}_{ij} - \sum_{j=1}^N U'(\|\mathbf{Q}\mathbf{r}_{ij}\|) \frac{\mathbf{Q}\mathbf{r}_{ij}}{\|\mathbf{Q}\mathbf{r}_{ij}\|} \\
&= \mathbf{Q} \left( - \sum_{j=1}^N \dot{\mathbf{r}}_{ij} - \sum_{j=1}^N \nabla U(\|\mathbf{r}_{ij}\|) \right) \\
&= \mathbf{Q}\mathbf{a}_i(\mathbf{X}, \dot{\mathbf{X}}).
\end{aligned}$$

Existing ML models, like TDAGNN, do not satisfy these symmetries.

#### 4 Equivariant controllers for learning decentralized flocking

In this section, we present a rotation equivariant ML controller for decentralized flocking. Our approach replaces the CNN in TDAGNN with an  $\text{O}(2)$  equivariant CNN, ensuring rotation and reflection equivariance of the resulting ML controller.

##### 4.1 Rotation equivariant convolution layers

TDAGNN is translation invariant, but not rotation equivariant because its CNN component  $\phi$  is not. There has been significant effort put toward developing roto-translation equivariant CNNs (e.g.,  $\text{SO}(2)$ -steerable CNNs [39]); however, these cannot be directly integrated into TDAGNN. As such, we aim to replace  $\phi$  with an  $\text{O}(2)$  equivariant CNN  $\phi_{\text{EqConv}}$  equipped with rotation equivariant convolutional layers and activations. To ease our presentation, we make the following two assumptions:

**Assumption 1** *The 1D convolutional layers*

$$\{\text{Conv1d}_\ell : \mathbb{R}^{C_\ell \times F_\ell} \rightarrow \mathbb{R}^{C_{\ell+1} \times F_{\ell+1}}\}_{\ell=1}^{L_\phi}$$

of  $\phi$  have no padding.

**Assumption 2** *The input of  $\phi$  always has the same size.*

We represent the input  $\mathbf{H}_{i,\ell}$  of  $\text{Conv1d}_\ell$  as a block matrix composing vectors in  $\mathbb{R}^2$  that are  $O(2)$  equivariant with respect to the agents' positions and velocities:

$$\mathbf{H}_{i,\ell} = [\mathbf{g}_{c_{in},f}]_{c_{in}=1,f=1}^{(C_\ell/2),F_\ell} \subset \mathbb{R}^{C_\ell \times F_\ell}$$

If  $\ell = 1$  and we use  $\psi$  from Eqn. (5), then  $\mathbf{H}_{i,\ell} = \mathbf{H}_i$  from section 3.4,  $C_\ell = 6$ , and  $F_\ell = K$ . Moreover, the last convolutional layer in  $\phi$  outputs acceleration so  $C_{L_\phi+1} = 2$  and  $F_{L_\phi+1} = 1$ . By Assumption 1,  $\text{Conv1d}_\ell$  can be represented by a collection of Toeplitz matrices  $\mathbf{W} : \{1, \dots, C_\ell\} \times \{1, \dots, C_{\ell+1}\} \rightarrow \mathbb{R}^{F_\ell \times F_{\ell+1}}$  and bias terms  $b : \{1, \dots, C_{\ell+1}\} \rightarrow \mathbb{R}$ . For  $c_{out} \in \{1, \dots, C_{\ell+1}\}$ , the output channel  $\text{Conv1d}_\ell(\mathbf{H}_{i,\ell})[c_{out}]$  can be represented as

$$\begin{aligned} & \text{Conv1d}_\ell(\mathbf{H}_{i,\ell})[c_{out}] \\ &= b(c_{out}) \mathbf{1}_{F_{\ell+1}}^\top + \sum_{c_{in}=1}^{C_\ell} [(\mathbf{H}_{i,\ell})_{c_{in},1}, \dots, (\mathbf{H}_{i,\ell})_{c_{in},F_\ell}] \mathbf{W}(c_{in}, c_{out}) \\ &= b(c_{out}) \mathbf{1}_{F_{\ell+1}}^\top + \sum_{c_{in}=1}^{C_\ell/2} \sum_{c=1}^2 [(\mathbf{g}_{c_{in},1})_c, \dots, (\mathbf{g}_{c_{in},F_\ell})_c] \mathbf{W}(2(c_{in}-1) + c, c_{out}) \\ &= b(c_{out}) \mathbf{1}_{F_{\ell+1}}^\top + \sum_{c_{in}=1}^{C_\ell/2} \mathbf{1}_2^\top \left[ [(\mathbf{g}_{c_{in},1})_1, \dots, (\mathbf{g}_{c_{in},F_\ell})_1] \mathbf{W}(2(c_{in}-1) + 1, c_{out}) \right. \\ & \quad \left. [(\mathbf{g}_{c_{in},1})_2, \dots, (\mathbf{g}_{c_{in},F_\ell})_2] \mathbf{W}(2(c_{in}-1) + 2, c_{out}) \right]. \end{aligned}$$

Applying an orthogonal matrix  $\mathbf{Q} \in O(2)$  to the agents' position and velocity, we have

$$\begin{aligned} & \text{Conv1d}_\ell \left( [\mathbf{Q}\mathbf{g}_{c_{in},f}]_{c_{in}=1,f=1}^{(C_\ell/2),F_\ell} \right) [c_{out}] \\ &= b(c_{out}) \mathbf{1}_{F_{\ell+1}}^\top + \sum_{c_{in}=1}^{C_\ell/2} \mathbf{1}_2^\top \left[ [(\mathbf{Q}\mathbf{g}_{c_{in},1})_1, \dots, (\mathbf{Q}\mathbf{g}_{c_{in},F_\ell})_1] \mathbf{W}(2(c_{in}-1) + 1, c_{out}) \right. \\ & \quad \left. [(\mathbf{Q}\mathbf{g}_{c_{in},1})_2, \dots, (\mathbf{Q}\mathbf{g}_{c_{in},F_\ell})_2] \mathbf{W}(2(c_{in}-1) + 2, c_{out}) \right] \\ & \neq \mathbf{Q} \text{Conv1d}_\ell \left( [\mathbf{g}_{c_{in},f}]_{c_{in}=1,f=1}^{(C_\ell/2),F_\ell} \right). \end{aligned}$$

From the above analysis, we see that  $\text{Conv1d}_\ell$  is **not**  $O(2)$  **equivariant** for three reasons: (1) the bias term, (2) vector element indexing is not  $O(2)$  equivariant, and (3)  $\mathbf{Q}$  does not commute with  $\mathbf{1}_2^\top$ . We need to address these issues to develop an  $O(2)$  equivariant convolution. For the first issue, we

eliminate the bias term. For the second issue, we eliminate the vector element indexing through weight sharing. By setting  $\mathbf{W}(2(c_{\text{in}} - 1) + 1, c_{\text{out}}) = \mathbf{W}(2(c_{\text{in}} - 1) + 2, c_{\text{out}})$  for all  $c_{\text{in}}$ , then for an output channel  $c_{\text{out}}$ , we have

$$\begin{aligned} & \sum_{c_{\text{in}}=1}^{C_{\ell}/2} \mathbf{1}_2^{\top} \left[ [(\mathbf{g}_{c_{\text{in}},1})_1, \dots, (\mathbf{g}_{c_{\text{in}},F_{\ell}})_1] \mathbf{W}(2(c_{\text{in}} - 1) + 1, c_{\text{out}}) \right] \\ & \quad \left[ [(\mathbf{g}_{c_{\text{in}},1})_2, \dots, (\mathbf{g}_{c_{\text{in}},F_{\ell}})_2] \mathbf{W}(2(c_{\text{in}} - 1) + 2, c_{\text{out}}) \right] \\ & = \sum_{c_{\text{in}}=1}^{C_{\ell}/2} \mathbf{1}_2^{\top} [\mathbf{g}_{c_{\text{in}},1}, \dots, \mathbf{g}_{c_{\text{in}},F_{\ell}}] \mathbf{W}(2(c_{\text{in}} - 1) + 1, c_{\text{out}}). \end{aligned}$$

For the third issue, we drop  $\mathbf{1}_2^{\top}$ , which changes the number of rows per output channel from one to two. To retain the original number of rows in the output of Conv1d, we halve the number of output channels but set each output channel to have two rows (or ‘‘subchannels’’). With these changes, we define a new  $O(2)$  equivariant convolution EqConv $_{\ell}$ : For output channels  $c_{\text{out}} \in \{1, \dots, C_{\ell+1}/2\}$ ,

$$\text{EqConv}_{\ell}(\mathbf{H}_{i,\ell})[c_{\text{out}}] = \sum_{c_{\text{in}}=1}^{C_{\ell}/2} [\mathbf{g}_{c_{\text{in}},1}, \dots, \mathbf{g}_{c_{\text{in}},F_{\ell}}] \mathbf{W}(2(c_{\text{in}} - 1) + 1, c_{\text{out}}).$$

EqConv $_{\ell}$  is  $O(2)$  equivariant since

$$\begin{aligned} & \text{EqConv}_{\ell} \left( [\mathbf{Q}\mathbf{g}_{c_{\text{in}},f}]_{c_{\text{in}}=1,f=1}^{(C_{\ell}/2),F_{\ell}} \right) [c_{\text{out}}] \\ & = \sum_{c_{\text{in}}=1}^{C_{\ell}/2} [\mathbf{Q}\mathbf{g}_{c_{\text{in}},1}, \dots, \mathbf{Q}\mathbf{g}_{c_{\text{in}},F_{\ell}}] \mathbf{W}(2(c_{\text{in}} - 1) + 1, c_{\text{out}}) \\ & = \mathbf{Q} \text{EqConv}_{\ell} \left( [\mathbf{g}_{c_{\text{in}},f}]_{c_{\text{in}}=1,f=1}^{(C_{\ell}/2),F_{\ell}} \right) [c_{\text{out}}]. \end{aligned}$$

EqConv $_{\ell}$  can be implemented using a standard 2D convolutional layer whose kernels have one row and a vertical stride of one.

## 4.2 Rotation equivariant activations

To build an  $O(2)$  equivariant CNN, we need  $O(2)$  equivariant activations. Notice that the output of EqConv $_{\ell}$  is also a block matrix composing 2D vectors that are  $O(2)$  equivariant:

$$\mathbf{H}_{i,\ell+1} = \text{EqConv}_{\ell}(\mathbf{H}_{i,\ell}) = [\mathbf{g}_{c_{\text{out}},f}]_{c_{\text{out}}=1,f=1}^{(C_{\ell+1}/2),F_{\ell+1}} \subset \mathbb{R}^{C_{\ell+1} \times F_{\ell+1}}.$$

We construct an  $O(2)$  equivariant activation for  $\mathbf{H}_{i,\ell+1}$  by applying an  $O(2)$  equivariant activation to each  $\mathbf{g}_{c_{\text{out}},f}$  separately. By Proposition 1 of [21], any  $O(2)$  equivariant function can be expressed as  $\sigma(\mathbf{x}) = \mathbf{x}\tilde{\sigma}(\|\mathbf{x}\|)$  for some function  $\tilde{\sigma} : \mathbb{R} \rightarrow \mathbb{R}$ . Therefore, the output channel  $c_{\text{out}} \in \{1, \dots, C_{\ell+1}/2\}$  with an equivariant activation applied is given by

$$\begin{aligned} \sigma(\mathbf{H}_{i,\ell+1})[c_{\text{out}}] & = [\sigma(\mathbf{g}_{c_{\text{out}},1}), \dots, \sigma(\mathbf{g}_{c_{\text{out}},F_{\ell+1}})] \\ & = \mathbf{H}_{i,\ell+1}[c_{\text{out}}] \odot \mathbf{1}_2 [\tilde{\sigma}(\|\mathbf{g}_{c_{\text{out}},1}\|), \dots, \tilde{\sigma}(\|\mathbf{g}_{c_{\text{out}},F_{\ell+1}}\|)], \end{aligned}$$

where  $\odot$  denotes the Hadamard product. The  $O(2)$  equivariant convolution layer and  $O(2)$  equivariant activations are combined to create an  $O(2)$  equivariant convolution neural network  $\phi_{\text{EqConv}}$ .

We construct the following tailored activations for our application:

$$\tilde{\sigma}_{\text{ln}}(x) = \begin{cases} 1 & x = 0 \\ \frac{\ln(1+x)}{x} & x \neq 0 \end{cases}, \quad \text{and } \tilde{\sigma}_{\text{tanh}}(x) = \tanh(x),$$

$$\sigma_{\text{ln}}(\mathbf{H}_{i,\ell}[c_{\text{out}}]) = \mathbf{H}_{i,\ell}[c_{\text{out}}] \odot \mathbf{1}_2[\tilde{\sigma}_{\text{ln}}(\|\mathbf{g}_{c_{\text{out},1}\|}, \dots, \tilde{\sigma}_{\text{ln}}(\|\mathbf{g}_{c_{\text{out},F_{\ell+1}}\|})],$$

$$\sigma_{\text{tanh}}(\mathbf{H}_{i,\ell}[c_{\text{out}}]) = \mathbf{H}_{i,\ell}[c_{\text{out}}] \odot \mathbf{1}_2[\tilde{\sigma}_{\text{tanh}}(\|\mathbf{g}_{c_{\text{out},1}\|}, \dots, \tilde{\sigma}_{\text{tanh}}(\|\mathbf{g}_{c_{\text{out},F_{\ell+1}}\|})].$$

The activation  $\sigma_{\text{ln}}$  provides an important normalization effect similar to tanh in the non-equivariant ML controller TDAGNN. Large convolutional layer inputs can occur because the input features in Eqn. (5) are unbounded as  $\|\mathbf{r}_{ij}\| \rightarrow 0$ , potentially causing instabilities during training. Applying tanh elementwise bounds the features passed inside the CNN to  $(-1, 1)$ . However, in the non-equivariant controllers, tanh is not applied before the first convolutional layer because it reduces all large-magnitude features to approximately the same magnitude (i.e., it is saturated); doing so would remove important information about the proximity of neighboring agents. Unfortunately, the first convolutional layer is still subject to large inputs. In contrast, for  $\phi_{\text{EqConv}}$  we can reduce the size of the inputs to the first convolutional layer and avoid saturation by using  $\sigma_{\text{ln}}$ . Next, the activation  $\sigma_{\text{tanh}}$  is simply a nonlinear scaling of the feature vectors.

### 4.3 Further improving TDAGNN

We present two strategies to improve both equivariant and non-equivariant ML controllers further.

**Activate once:** The tanh activation of the CNN  $\phi$  normalizes the output of each convolutional layer into  $(-1, 1)$ . Since the activation is applied after all but the last convolutional layer, the last convolutional layer must have large weights to ensure the controller can output a large acceleration vector. A large acceleration is needed whenever the controller needs to react quickly to maintain a connected communication graph or avoid collision. However, large weights concentrated in the last convolutional layer may cause the controller to output large accelerations too often, leading to over-corrections of the agents' velocities. When training TDAGNN, the CNN  $\phi$  must balance the need for large weights in the last convolutional layer with their risk. This challenge is lessened by applying the activation only after the first convolutional layer, allowing the controller to learn large weights across its convolutional layers.

**Mean one-hop aggregation:** In Eqn. (2), TDAGNN uses a sum aggregation of the messages in the one-hop neighborhood of agent  $i$ . Sum aggregation can cause over-corrections when agent  $i$ 's neighbors send similar messages. Consider the scenario where all neighbors of agent  $i$  have the same velocity  $\mathbf{v}_{\mathcal{N}_i}$  and agent  $i$  has velocity  $\dot{\mathbf{x}}_i \neq \mathbf{v}_{\mathcal{N}_i}$ . Each neighbor sends a message to

agent  $i$  requesting that it corrects its velocity by  $-(\dot{\mathbf{x}}_i - \mathbf{v}_{\mathcal{N}_i})$ . With sum aggregation, agent  $i$  overcorrects its velocity by  $-|\mathcal{N}_i|(\dot{\mathbf{x}}_i - \mathbf{v}_{\mathcal{N}_i})$ , but with mean aggregation, agent  $i$  corrects its velocity by  $-(\dot{\mathbf{x}}_i - \mathbf{v}_{\mathcal{N}_i})$ , exactly what was requested by all its neighbors.

## 5 Generalization analysis

In this section, we analyze the generalizability of TDAGNN-related models when trained for flocking following the generalization analysis framework in [18].

### 5.1 Generalization gap

**Definition 3 (Generalization gap)** Let  $f : \mathcal{X} \rightarrow \mathcal{Y}$  and define the loss function  $\mathcal{L} : \mathcal{Y} \times \mathcal{Y} \rightarrow [0, \infty)$ . Let  $\mathcal{B} = \{(x_b, y_b)\}_{b=1}^B$  be a set of i.i.d. samples from a probability distribution  $\mathcal{D}$  over  $\mathcal{X} \times \mathcal{Y}$ . The *generalization gap*  $\mathcal{R}_{\mathcal{B}, \mathcal{L}}$  of  $f$  is the difference between the expected risk and empirical risk, i.e.,

$$\mathcal{R}_{\mathcal{B}, \mathcal{L}}(f) = \underbrace{\mathbb{E}_{(x, y) \sim \mathcal{D}}[\mathcal{L}(f(x), y)]}_{\text{expected risk}} - \underbrace{\frac{1}{B} \sum_{b=1}^B \mathcal{L}(f(x_b), y_b)}_{\text{empirical risk}}.$$

The generalization gap can be bounded by the expressiveness of the class of ML models. Empirical Rademacher complexity (ERC) measures how well the family of functions can fit random noise.

**Definition 4 (Empirical Rademacher complexity)** Let  $\mathcal{F} = \{f : \mathcal{X} \rightarrow \mathbb{R}\}$  be a family of bounded functions and  $\mathcal{B} = \{x_b\}_{b=1}^B \subset \mathcal{X}$ . The *empirical Rademacher complexity* (ERC) of  $\mathcal{F}$  is

$$\hat{\mathfrak{R}}_{\mathcal{B}}(\mathcal{F}) = \mathbb{E}_{\boldsymbol{\sigma}} \left[ \sup_{f \in \mathcal{F}} \frac{1}{B} \sum_{b=1}^B (\boldsymbol{\sigma})_b f(x_b) \right],$$

where the entries of  $\boldsymbol{\sigma} \in \{-1, 1\}^B$  are distributed such that  $P((\boldsymbol{\sigma})_b = -1) = 1/2$  and  $P((\boldsymbol{\sigma})_b = 1) = 1/2$ .

Using the ERC, a probabilistic bound for the generalization gap can be derived.

**Theorem 3 (ERC bounds generalization gap [23])** Define the loss function  $\mathcal{L} : \mathcal{Y} \times \mathcal{Y} \rightarrow [0, 1]$ , let  $\mathcal{F} = \{f : \mathcal{X} \rightarrow \mathcal{Y}\}$ , and let  $\mathcal{D}$  be a probability distribution over  $\mathcal{X} \times \mathcal{Y}$ . Let  $\mathcal{B} = \{(x_b, y_b)\}_{b=1}^B$  be a set of i.i.d. samples from  $\mathcal{D}$ . For any  $\delta > 0$ , for all  $f \in \mathcal{F}$ , the following bound holds with probability  $1 - \delta$ :

$$\mathcal{R}_{\mathcal{B}, \mathcal{L}}(f) \leq 2\hat{\mathfrak{R}}_{\mathcal{B}}(\mathcal{F}_{\mathcal{L}}) + 3\sqrt{\frac{\ln(\frac{2}{\delta})}{2B}},$$

where  $\mathcal{F}_{\mathcal{L}} = \{(x, y) \mapsto \mathcal{L}(f(x), y) : f \in \mathcal{F}\}$ .

Therefore, we only need to bound ERC. The covering number is a celebrated tool to bound ERC.

**Definition 5 (Covering number)** The covering number  $\mathcal{N}(\mathcal{Z}, r, \|\cdot\|)$  of a set  $\mathcal{Z}$  with respect to some norm  $\|\cdot\|$  is the minimum cardinality of a set  $\mathcal{Z}'$  such that, for any element of  $\mathcal{Z}$ , there is an element in  $\mathcal{Z}'$  that is within a distance  $r$  of it, i.e.,  $\mathcal{N}(\mathcal{Z}, r, \|\cdot\|) = \min\{|\mathcal{Z}'| : \forall z \in \mathcal{Z}, \exists z' \in \mathcal{Z}', \|z - z'\| \leq r\}$ .

Now, we state an established bound of the ERC in terms of the covering number.

**Lemma 1 (Bounding ERC [3])** Let  $\mathcal{F} = \{f : \mathcal{X} \rightarrow [-\beta, \beta]\}$ , and assume that there exists a function  $f_0 \in \mathcal{F}$  such that  $f_0(x) = 0$  for all  $x \in \mathcal{X}$ . With  $\|f\|_\infty = \sup_{x \in \mathcal{X}} |f(x)|$ , for any  $\mathcal{B} = \{x_i\}_{i=1}^B \subset \mathcal{X}$ ,

$$\hat{\mathfrak{R}}_{\mathcal{B}}(\mathcal{F}) \leq \inf_{\alpha > 0} \left( \frac{4\alpha}{\sqrt{B}} + \frac{12}{B} \int_{\alpha}^{2\beta\sqrt{B}} \sqrt{\ln(\mathcal{N}(\mathcal{F}, r, \|\cdot\|_\infty))} dr \right).$$

## 5.2 Behavior cloning with fast-forwarding

The space of training data for TDAGNN – using IL with DAgger – is the set of tuples  $(\mathbf{X}, \dot{\mathbf{X}}, \{\mathbf{H}_i\}_{i=1}^N)$ , and the probability distribution on that space is induced by how DAgger generates these tuples. However, Definition 3 requires that the training samples are independent, but the tuples generated by DAgger are not for two reasons. First, each tuple is computed using the previously generated tuple. At the beginning of each epoch, flocking is simulated for  $T$  time steps where  $(\mathbf{X}(t_{n+1}), \dot{\mathbf{X}}(t_{n+1}))$  is computed by applying an acceleration to  $(\mathbf{X}(t_n), \dot{\mathbf{X}}(t_n))$ . In addition,  $\mathbf{H}_i(t_n)$  is computed using  $\{(\mathbf{X}(t_{n-k+1}), \dot{\mathbf{X}}(t_{n-k+1}))\}_{k=1}^K$ . The second reason is that the ML controller is trained on previously generated tuples, and it can influence what tuples are generated next by applying its acceleration.

The second reason cannot be addressed without fundamentally changing DAgger, and therefore, the probability distribution it induces on the space of training data. A primary motivation for the DAgger algorithm is allowing the ML controller to influence what training examples (e.g., tuples) are generated, and since the ML controller’s weights depend on previously generated training examples, the training examples generated next cannot be independent. Therefore, we cannot analyze the generalization gap of ML controllers trained using IL with DAgger. To move forward with our analysis, we substitute DAgger with a variation of behavior cloning we call **fast-forward behavior cloning** (FFBC).

FFBC addresses the second reason by only using the expert controller’s acceleration during the flocking simulations run before each epoch. The first reason is addressed by ensuring every tuple saved is derived from a newly sampled flock initial condition using fast-forwarding. Instead of sampling an initial

condition once at the beginning of each simulation, we sample an initial condition at each time step of the simulation. At time  $t_n$ , we sample  $(\mathbf{X}(0), \dot{\mathbf{X}}(0))$ , and then use the expert controller to advance it to  $(\mathbf{X}(t_n), \dot{\mathbf{X}}(t_n))$  by sequentially applying the accelerations  $\{\mathbf{a}_i(\mathbf{X}(t_{n'}), \dot{\mathbf{X}}(t_{n'}))\}_{n'=0}^{n-1}$ . Once the last acceleration is applied, we have also computed  $\{\mathbf{H}_i(t_n)\}_{i=1}^N$ . Finally, we save the tuple  $(\mathbf{X}(t_n), \dot{\mathbf{X}}(t_n), \{\mathbf{H}_i(t_n)\}_{i=1}^N)$  to the training set.

FFBC is independent of the ML controller’s weights, so the dataset of tuples may be computed before training by running  $E$  flocking simulations. Note that the dataset is dependent on whether the ML controller uses sum aggregation or mean aggregation (see section 4.3) because the tuples contain  $\mathbf{H}_i$ . The datasets are split into training and test sets, and each ML controller is trained on its respective training set. We train the ML controller on the entire training set each epoch so that the training set size does not vary as the ML controller trains, allowing us to compare generalization gaps at different epochs.

### 5.3 TDAGNN reinterpretations and loss function

The bound proved in [18] is for EGNN [33] applied to graph-level tasks (e.g., graph classification). For these tasks, all *invariant* node features after the last EGNN layer are aggregated, and the aggregated feature is fed to a final scoring model (e.g., an MLP) to produce a label for the graph. In flocking, each agent attempts to compute an acceleration for itself to match that of an expert controller, so the ML controller is performing a node-level task. We need to convert the node-level task into a graph-level task to adapt the analysis in [18]. We normally train ML controllers using squared error (SE) between their acceleration and the expert’s acceleration averaged over all agents, resulting in a mean SE (MSE) loss. To convert to a graph-level task, we modify the output of each agent to be the SE instead of its acceleration, then define the scoring model  $h_G$  for the flock as

$$h_G(\text{MSE}) = w^2 + \text{MSE}, \quad (7)$$

where  $\text{MSE} = \frac{1}{N} \sum_{i=1}^N \text{SE}_i$ ,  $\text{SE}_i = \|\mathbf{a}_i(\mathbf{X}, \dot{\mathbf{X}}) - \phi(\mathbf{H}_i)\|^2$ , and  $w$  is a trainable parameter in the scoring model. Note that  $\text{SE}_i$  is  $O(2)$  invariant, so MSE is an aggregation of invariant node features. The scoring model now computes the original loss given by Eqn. (9), so we can simply choose the identity function  $\mathcal{L}(y) = y$  as the loss function. However, to comply with the assumptions of Theorem 3, we instead choose the loss function  $\mathcal{L}(y) = \min\{1, y/C\}$  for some  $C > 0$ .

### 5.4 Bounding the generalization gap

Paper [18] uses MLPs to update the node features of EGNN, so our adaptation of their proof considers the MLP representations of  $\phi$  given by Lemma 8 or

9. The authors also assume that the input to EGNN is bounded, so we also assume a bound on the input of the MLP representation in Assumption 4.

**Definition 6 (Input of TDAGNN as an MLP)** The first convolutional layer  $\text{Conv1d}_1 : \mathbb{R}^{C_1 \times F_1} \rightarrow \mathbb{R}^{C_2 \times F_2}$  of  $\phi$  has  $C_1$  input channels that are row vectors of the form  $\mathbf{H}_{i,1}[c_{\text{in}}] = [(\mathbf{H}_i)_{c_{\text{in}},1}, \dots, (\mathbf{H}_i)_{c_{\text{in}},F_1}]$ . The input  $\mathbf{H}_{i,1}^{\text{MLP}}$  of  $\phi$  as an MLP is the row-wise concatenation of the input channels and  $\mathbf{1}_{F_2}^\top$  to account for the bias term of  $\text{Conv1d}_1$ :  $\mathbf{H}_{i,1}^{\text{MLP}} = [\mathbf{H}_{i,1}[1], \dots, \mathbf{H}_{i,1}[C_\ell], \mathbf{1}_{F_2}^\top]$ .

**Definition 7 (Input of O(2) equivariant TDAGNN as an MLP)**  $\text{EqConv}_1 : \mathbb{R}^{C_1 \times F_1} \rightarrow \mathbb{R}^{C_2 \times F_2}$  of  $\phi_{\text{EqConv}}$  has  $C_1/2$  input channels that are two-row matrices of the form  $\mathbf{H}_{i,1}[c_{\text{in}}] = [\mathbf{g}_{c_{\text{in}},1}, \dots, \mathbf{g}_{c_{\text{in}},F_1}]$ . The input  $\mathbf{H}_{i,1}^{\text{MLP}}$  of  $\phi$  as an MLP is the row-wise concatenation of the input channels:  $\mathbf{H}_{i,1}^{\text{MLP}} = [\mathbf{H}_{i,1}[1], \dots, \mathbf{H}_{i,1}[C_1/2]]$ .

**Assumption 4 (FFBC datasets are bounded)** *There exists  $\beta \geq 1$  such that for all tuples  $(\mathbf{X}, \dot{\mathbf{X}}, \{\mathbf{H}_i\}_{i=1}^N)$  in the FFBC dataset,*

$$\max_i \{ \|\mathbf{a}_i(\mathbf{X}, \dot{\mathbf{X}})\|, \|\mathbf{H}_{i,1}^{\text{MLP}}\|_F \} \leq \beta,$$

where  $\mathbf{a}_i$  is the expert controller and  $\mathbf{H}_{i,1}^{\text{MLP}}$  is defined in either Definition 6 or Definition 7.

Now we state the generalization gap bound for the ML controllers with proof in the appendix.

**Proposition 1 (Generalization bound of TDAGNN)** *Let  $P$  be the probability distribution over tuples  $(\mathbf{X}, \dot{\mathbf{X}}, \{\mathbf{H}_i\}_{i=1}^N)$  induced by FFBC. Let  $\mathcal{L}(y) = \min\{1, y/C\}$  for  $C > 0$  be the loss function. Let  $\{\mathbf{W}_\ell\}_{\ell=1}^{L_\phi}$  be the weights of the MLP representation  $\Phi$  of  $\phi$  given by Lemma 8 or 9, and let  $w$  of  $h_G$  in Eqn. (7) be such that  $w \in [0, \sqrt{C}]$ . For any  $\delta > 0$ , with probability at least  $1 - \delta$  over choosing a batch  $\mathcal{B}$  of  $B$  tuples sampled from  $P$ , the following bound holds:*

$$\begin{aligned} \mathcal{R}_{\mathcal{B}, \mathcal{L}}(h_G) &\leq \frac{8}{B} + \\ &\frac{48d}{\sqrt{B}} \sqrt{(3L_\phi + 1) \ln(10L_\phi \beta K_\sigma^{L_\phi} \sqrt{dBC}) + (2L_\phi + 3) \sum_{\ell=1}^{L_\phi} \ln(\max\{1, \|\mathbf{W}_\ell\|_F\})} + \\ &3 \sqrt{\frac{\ln(\frac{2}{\delta})}{2B}}. \end{aligned} \tag{8}$$



## 6 Experiments

**Controllers and hyperparameters:** We compare four ML controllers and the expert controller used to train them. The expert controller is TannerEtAl from Eqn. (1) with the potential function from Eqn. (4). In [37], TannerEtAl’s acceleration  $\mathbf{a}_i(\mathbf{X}, \dot{\mathbf{X}})$  is clamped so that  $\|\mathbf{a}_i(\mathbf{X}, \dot{\mathbf{X}})\|_\infty \leq 100$ , but this breaks TannerEtAl’s  $O(2)$  equivariance. To retain  $O(2)$  equivariance, we enforce  $\|\mathbf{a}_i(\mathbf{X}, \dot{\mathbf{X}})\|_2 \leq 100$ .

| Controller       | Aggregation | Activations (after conv. $\ell$ )                        | Conv. layers |
|------------------|-------------|--|--------------|
| TDAGNN           | Sum         | $\sigma_\ell = \tanh, \ell \in \{1, \dots, L_\phi - 1\}$ | Conv1d       |
| TDAGNN+TF        | Sum         | $\sigma_1 = \tanh$                                       | Conv1d       |
| TDAGNN+TF+ $\mu$ | Mean        | $\sigma_1 = \tanh$                                       | Conv1d       |
| ETDAGNN          | Mean        | $\sigma_0 = \sigma_{\ln}, \sigma_1 = \sigma_{\tanh}$     | EqConv       |

Table 1: Summary of the architectural differences between the compared ML controllers for flocking. The subscripts  $\ell$  of the activations in the Activations column indicate the convolutional layer that the activation is applied after. If the subscript  $\ell$  is 0, then the activation is applied before the first convolutional layer. If a subscript value is not listed, then no (or the identity) activation is applied after the corresponding convolutional layer.

The first controller is TDAGNN from [37] and serves as a baseline. The second is TDAGNN with the “Activate once” improvement described in section 4.3 and is denoted by TDAGNN+TF – “TF” stands for “tanh first.” The third is TDAGNN with both the improvements described in section 4.3 and is denoted by TDAGNN+TF+ $\mu$ . The last is TDAGNN+TF+ $\mu$  with the CNN  $\phi_{\text{EqConv}}$  described in section 4.1 and the equivariant activations proposed in section 4.2, and it is denoted by ETDAGNN. The architectural differences, including what activations are used after each convolutional layer, are summarized in Table 1. All ML controllers use  $L_\phi = 3$  convolutional layers mapping  $\mathbb{R}^{C_\ell \times F_\ell}$  to  $\mathbb{R}^{C_{\ell+1} \times F_{\ell+1}}$  for  $\ell \in \{1, \dots, L_\phi\}$ . Explicitly writing their domains and ranges,  $(C_1, F_1) = (6, K)$ ,  $(C_2, F_2) = (32, 1)$ ,  $(C_3, F_3) = (32, 1)$ , and  $(C_4, F_4) = (2, 1)$ . With these hyperparameters, Table 2 shows each ML controller’s trainable parameter count.

|                 | <i>TDAGNN</i> | <i>TDAGNN+TF</i> | <i>TDAGNN+TF+<math>\mu</math></i> | <i>ETDAGNN</i> |
|-----------------|---------------|------------------|-----------------------------------|----------------|
| <b>#Weights</b> | 1,730         | 1,730            | 1,730                             | 416            |

Table 2: Number of trainable weights of the ML controllers for decentralized flocking.

**Training:** All ML controllers are trained for flocking control using IL with DAgger for  $E = 400$  epochs and then tested in flocking, leader following, and obstacle avoidance scenarios. We initialize  $\beta_0 = \beta_{\text{init}} = 0.993$ , and set  $\beta_e = \max\{\beta_{e-1}\beta_{\text{init}}, 0.5\}$ . Tuples are generated and added to the training set by running flocking simulations for  $T = 2/\Delta t$  time steps with  $\Delta t = 10^{-2}$ . The initial condition for each simulation is sampled from a dataset of initial conditions. The training set of tuples is capped at 10,000 examples, and the oldest examples are discarded first after reaching the cap. After the flocking simulation of each epoch, we sample 200 batches of 20 tuples with replacement from the training set. For each batch, we compute the loss averaged over the batch and update the ML controller’s weights. The loss function for one tuple is

$$\mathcal{L}(\mathbf{X}, \dot{\mathbf{X}}, \{\mathbf{H}_i\}_{i=1}^N) = \frac{1}{N} \sum_{i=1}^N \|\mathbf{a}_i(\mathbf{X}, \dot{\mathbf{X}}) - \phi(\mathbf{H}_i)\|^2. \quad (9)$$

The trainable parameters are initialized using Xavier uniform initialization with gain 1, and optimized using the Adam optimizer with learning rate  $5 \times 10^{-5}$ ,  $\beta_1 = 0.9$ , and  $\beta_2 = 0.999$ .

**Initial conditions:** The dataset of flock initial conditions is randomly generated following the procedure described in [37]. We refer to this dataset as the *RandomDisk* dataset. Each initial condition composes  $N$  agents whose positions are distributed in a 2D disk of radius  $\sqrt{N}$ . Having radius  $\sqrt{N}$  implies that the ratio of the number of agents to the disk’s area is the constant  $\pi$ . The agents are placed in the disk uniformly randomly such that three conditions are met: the agents are not too close (for  $j \in \mathcal{N}_i(0)$ ,  $R_{\min} \leq \|\mathbf{r}_{ij}\| \leq R_{\text{comm}}$ ); the agents have enough neighbors ( $|\mathcal{N}_i(0)| \geq \text{deg}_{\min} \geq 0$ ); and, the flock’s communication graph is connected. The agents’ velocities are initialized to  $\dot{\mathbf{X}}(0) = \mathbf{V}_{\text{init}} + \mathbf{v}_{\text{bias}} \mathbf{1}_N^\top$  where the entries of  $\mathbf{V}_{\text{init}}$  and  $\mathbf{v}_{\text{bias}}$  are uniformly randomly sampled from  $[-v_{\max}, v_{\max}]$  for  $v_{\max} \in [0, \infty)$ . Fig. 2 shows example initial conditions of this dataset. Following [37], we choose the RandomDisk dataset parameters as  $N = 100$ ,  $R_{\min} = 0.1$ ,  $R_{\text{comm}} = 1$ ,  $\text{deg}_{\min} = 2$ , and  $v_{\max} = 3$ .

**Metrics:** We quantify the performance of the ML controllers using the two metrics:

- **Velocity variance:** The variance of velocities is  $\text{var}(\dot{\mathbf{x}}) = \frac{1}{N} \sum_{i=1}^N \|\dot{\mathbf{x}}_i - \text{mean}(\dot{\mathbf{x}})\|^2$  where  $\text{mean}(\dot{\mathbf{x}}) := \frac{1}{N} \sum_{i=1}^N \dot{\mathbf{x}}_i$ . Lower variance implies the flock is closer to a limiting velocity of asymptotic flocking.
- **Mean acceleration norm:** The mean acceleration norm of the agents is  $\frac{1}{N} \sum_{i=1}^N \|\ddot{\mathbf{x}}_i(t_n)\|$ . A lower mean acceleration norm means the controller uses a smaller control input to achieve its objective. This metric measures the controller’s efficiency because less acceleration implies less energy expenditure for the flock.

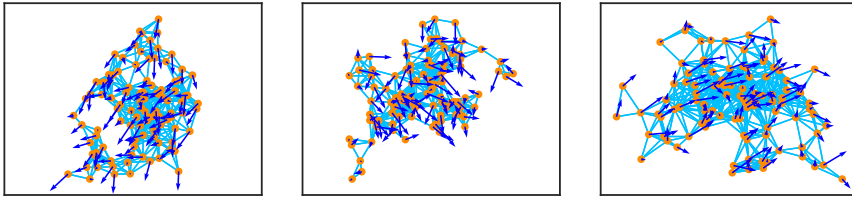


Fig. 2: Examples from the RandomDisk dataset of flock initial conditions. There are  $N = 100$  agents (orange dots) with at least  $\text{deg}_{\min} = 2$  neighbors (indicated by light blue edges connecting them). The distance between an agent and its neighbors is between  $R_{\min} = 0.1$  and  $R_{\text{comm}} = 1$ . The agents' velocities (dark blue arrows) have magnitudes no larger than  $2v_{\max} = 6$ .

### 6.1 Flocking

In this task, we observe significant performance gaps between TannerEtAl, the ML controllers using sum aggregation (TDAGNN and TDAGNN+TF+ $\mu$ ), and the ML controllers using mean aggregation (TDAGNN+TF+ $\mu$  and ETDAGNN). When presenting these results, we will compare these groups, and then compare the controllers within these groups when necessary. Keep in mind that ETDAGNN has 75% fewer trainable weights than other controllers (see Table 2).

For training, Fig. 3 shows the median Integral of the Velocity Variance (IVV) and the median Integral of the Mean Acceleration Norm (IMAN) on validation set of the RandomDisk dataset with  $N = 100$  and  $\Delta t = 10^{-2}$ . The mean-aggregation ML controllers achieve a lower median IVV and IMAN by epoch 80 than the sum-aggregation ML controllers do by epoch 400. Furthermore, at epoch 400, the IVV and IMAN IQRs of the best sum-aggregation ML controllers and worst mean-aggregation ML controllers do not overlap.

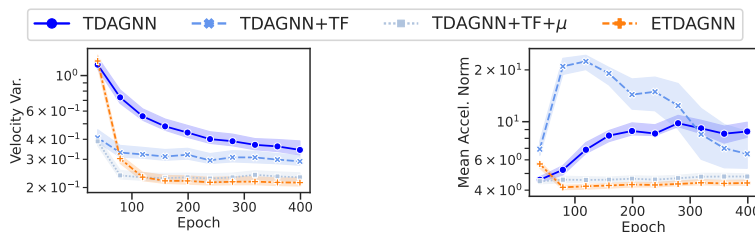


Fig. 3: Performance of ML controllers in flocking as they train. They are evaluated on the RandomDisk validation set with 100 agents. Each simulation is run for  $T = 2/\Delta t$  time steps where  $\Delta t = 10^{-2}$ . The curves show the median values of the respective metrics' integrals and the colored areas show their corresponding interquartile ranges.

For the sum-aggregation ML controllers, TDAGNN+TF has a lower median IVV than TDAGNN for all epochs. TDAGNN+TF has a higher IMAN than TDAGNN at epoch 40, and is over double compared to TDAGNN from epoch 80 to epoch 160. It takes until epoch 320 for it to become lower than TDAGNN. For the mean-aggregation ML controllers, at epoch 40, TDAGNN+TF+ $\mu$  has a median IVV less than half that of ETDAGNN, but ETDAGNN matches TDAGNN+TF+ $\mu$  by epoch 120. By epoch 400, the IVV of TDAGNN+TF+ $\mu$  is only larger than ETDAGNN by a few hundredths. At epoch 40, TDAGNN+TF+ $\mu$  also has a lower IMAN than ETDAGNN, but by epoch 80 and for the rest of the epochs, the IVV of TDAGNN+TF+ $\mu$  and ETDAGNN remain within that gap, both increasing at the same rate.

After training, we test each ML controller’s ability to achieve asymptotic flocking with separation on 50 RandomDisk initial conditions not used for training or hyperparameter tuning. We use  $N \in \{50, 100, 200, 400\}$  and  $\Delta t = 10^{-3}$ . Fig. 4 shows the median velocity variance over time. For all  $N$ , the mean-aggregation controllers reduce the velocity variance from about 4 to below 0.2 faster than the sum-aggregation controllers. When  $N \leq 100$ , the mean-aggregation ML controllers also reach a lower velocity variance at the last time step, but when  $N \geq 200$ , the sum-aggregation ML controllers reach a lower velocity variance. Surprisingly, when  $N = 50$ , the velocity variances of TannerEtAl and the mean-aggregation ML controllers are below that of TannerEtAl for the majority of the simulation. The exception is from times  $t_n \Delta t \in [0.1, 0.3]$  where TDAGNN+TF has a larger velocity variance than TannerEtAl. When  $N = 100$ , ETDAGNN reaches a lower velocity variance than TannerEtAl at the end of the simulation. Fig. 5 shows the median mean acceleration norm over time. The sum-aggregation ML controllers’ median mean acceleration norm at the last time step matches or is a few hundredths smaller than the mean-aggregation ML controllers.

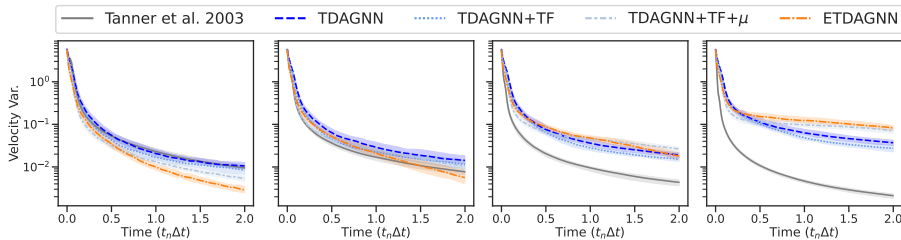


Fig. 4: Velocity variance of the controllers in flocking over the simulation time with time step size  $\Delta t = 10^{-3}$ . They are evaluated on the RandomDisk test set with the number of agents  $N \in \{50, 100, 200, 400\}$ . The lines show the median metric values and the colored areas show the corresponding interquartile ranges.

In summary, there is no best-performing ML controller for all tested flock sizes. For all tests, the mean-aggregation ML controllers reduce the velocity

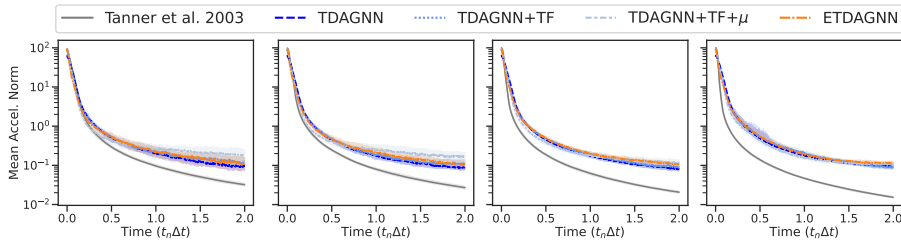


Fig. 5: Mean acceleration norm of the controllers in flocking over the simulation time with time step size  $\Delta t$ . They are evaluated on the RandomDisk test set with the number of agents  $N \in \{50, 100, 200, 400\}$ . The lines show the median metric values and the colored areas show the corresponding interquartile ranges.

variance of the flock faster than the sum-aggregation ones when the variance is large. The ML controller that reaches the smallest velocity variance by the last time step depends on  $N$ . When  $N \leq 100$ , ETDAGNN reaches the lowest variance at the last time step than other ML controllers. For larger  $N$ , TDAGNN+TF reaches the smallest velocity variance. The ML controllers have approximately the same mean acceleration norm. Animations of flocking are available on GitHub.<sup>2</sup>

## 6.2 Leader following

In leader following, the leader agents are selected from the flock and instructed to move along some predefined path (e.g., a line), and the other agents are followers. We test the ability of ML controllers, already trained for flocking, in conducting leader following using 50 RandomDisk initial conditions. Two agents from each initial condition are randomly selected to be leaders of the flock and the leaders' velocities are set equal. To prevent the followers from changing the leaders' trajectories, the leaders ignore all messages from the followers, i.e., the leaders only have directed edges from them to other agents. Consequently, the leaders do not pass on summaries of the messages they receive to their neighbors. In addition, the ML controllers only control the followers, and since the ML controllers are trained to maintain communication graph connectivity, the controllers are compelled to have the followers match the velocity of the leaders. The leader following simulations are run for  $T = 3/\Delta t$  time steps. In addition to the flocking validation metrics, leader following adds this validation metric:

- **Mean leader velocity distance (MLVD):** Let  $\mathbf{v}_{\text{ldr}}$  be the velocity of the leaders in the flock. We measure how close the flock is to the limiting velocity with  $\frac{1}{N} \sum_{i=1}^N \|\dot{\mathbf{x}}_i(t_n) - \mathbf{v}_{\text{ldr}}\|$ .

<sup>2</sup> Flocking animations: [github.com/Utah-Math-Data-Science/Equivariant-Decentralized-Controllers/tree/main/misc/animations/flocking](https://github.com/Utah-Math-Data-Science/Equivariant-Decentralized-Controllers/tree/main/misc/animations/flocking)

Fig. 6 shows the median MLVD and median mean acceleration norm over time. By the last time step, TDAGNN+TF+ $\mu$  has the lowest median MLVD. The medians of ETDAGNN and TDAGNN are nearly double and triple that of TDAGNN+TF+ $\mu$ . The ML controllers have approximately the same mean acceleration norm. Based on the performance of the ML controllers for the leader following task, we recommend TDAGNN+TF+ $\mu$  for the best performance; however, ETDAGNN provides comparable performance with 75% fewer trainable parameters. Animations of leader following are available on GitHub.<sup>3</sup>

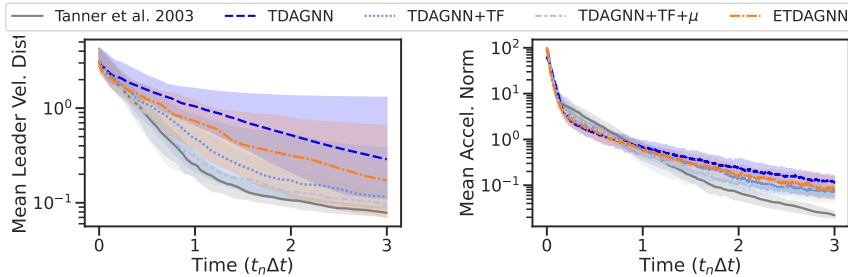


Fig. 6: Performance of controllers in leader following at each time step of the simulation. They are evaluated on the RandomDisk test set with  $N = 100$  agents where two agents are leaders.

### 6.3 Obstacle avoidance

When a flock is intercepting an obstacle, the ML controllers should have the flock circumnavigate it. For centralized flocking controllers, the primary requirement is that the agents do not collide with the obstacle. The centralized flocking controllers discussed can guarantee agent separation, which is readily extendable to obstacle collision avoidance if each agent can compute its distance from the obstacle. Decentralized flocking controllers, however, face the significant challenge of managing communication graph connectivity. An obstacle’s diameter can be larger than the communication radius  $R_{\text{comm}}$  of the agents, preventing agents on opposite sides of the obstacle from communicating. Decentralized flocking controllers have two options for successful circumnavigation – ensure that all agents move around the obstacle in the same direction, or devise a scheme that will guarantee communication graph connectivity is restored if groups of agents go around in different directions. We present a technique for helping decentralized flocking controllers conduct obstacle avoidance inspired by Fig. 2 of [30]. The technique is tested using disk-shaped obstacles with diameters up to nearly half of the flock’s diameter.

<sup>3</sup> Leader following animations: [github.com/Utah-Math-Data-Science/Equivariant-Decentralized-Controllers/tree/main/misc/animations/leader\\_following](https://github.com/Utah-Math-Data-Science/Equivariant-Decentralized-Controllers/tree/main/misc/animations/leader_following)

The obstacle avoidance dataset is built upon the RandomDisk dataset. For each initial condition, we construct a disk-shaped obstacle as follows. First, we place the center of a regular polygon with  $s$  sides of length  $R_{\min}$  relative to the flock such that two conditions are met:

1. **Polygon is in the middle:** Let  $\mathbf{x}_{i_*}$  and  $\mathbf{x}_{j_*}$  be agents whose distance is the diameter of the flock:  $\|\mathbf{r}_{i_*j_*}\| = \max_{i,j}\|\mathbf{r}_{ij}\|$ . The polygon's center is on the line passing through  $\text{mean}\{\mathbf{x}_{i_*}, \mathbf{x}_{j_*}\}$  that is perpendicular to the line passing through  $\mathbf{x}_{i_*}$  and  $\mathbf{x}_{j_*}$ .
2. **Polygon is in front:** At time zero, the minimum distance between the polygon center and the flock agents is greater than the polygon's circumradius plus  $R_{\text{comm}}$ .

The obstacle is the circumscribed circle of the polygon. Next, the agents need a mechanism to compute their position relative to the obstacle. In our simulation, we utilize the existing communication mechanism by placing additional *obstacle agents* on the vertices of the polygon. The obstacle agents only send their position to the flock agents. Moreover, the obstacle agents do not receive any messages from the flock agents; that is, the obstacle agents only have directed edges from them to the flock agents in the communication graph.

The final step is to randomly select two agents in the flock to be leaders (see section 6.2). Without leaders, the flock will not attempt to circumnavigate the obstacle; instead, the flock will turn around or simply halt in front of the obstacle. Leaders force the flock to continue past the obstacle. Leaders do not receive any messages from the obstacle agents. The leaders' velocity is fixed, so we select leaders that will always be at least  $R_{\min}$  away from the obstacle boundary. We set the initial velocity of leaders and followers to the unit vector pointing from  $\text{mean}\{\mathbf{x}_{i_*}, \mathbf{x}_{j_*}\}$  to the center of the obstacle. Examples are shown in Fig. 7.

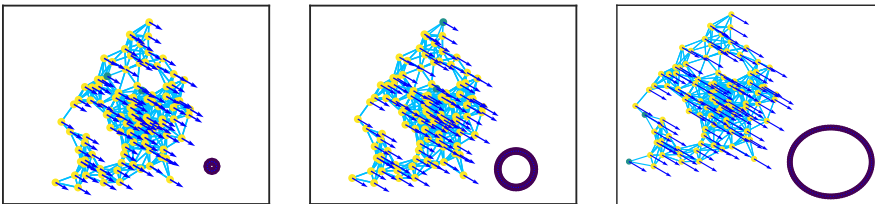


Fig. 7: Examples from the Obstacle Avoidance RandomDisk dataset of initial conditions of agents with  $\text{deg}_{\min} = 2$ ,  $R_{\min} = 0.1$ ,  $R_{\text{comm}} = 1$ , initial velocity (dark blue arrows) with magnitude 1, 98 agent followers (yellow), two leaders (green), and obstacles (purple) of perimeter 12, 48, and 96 (all multiplied by  $R_{\min}$ ).

Instead of terminating the obstacle avoidance simulations after some fixed number of time steps  $T$ , the simulations are run until any of the following three termination conditions are met:

1. **Disconnected communication graph:** First, check if the minimum distance between the flock and the obstacle is greater than  $R_{\text{comm}}$ , implying that the flock is unaware of the obstacle. If so, terminate the simulation if the communication graph containing leaders and followers is disconnected. Otherwise, terminate the simulation if the graph containing leaders, followers, and obstacle agents is disconnected.
2. **Collision:** Terminate the simulation if any flock agents are closer than  $R_{\text{min}}$  to each other or any obstacle agents, or the distance of any flock agent to the center of the obstacle is less than or equal to the radius of the obstacle.
3. **Obstacle passed:** Terminate the simulation if the minimum distance between the flock and obstacle agents has been less than  $R_{\text{comm}}$  for at least one step, and that distance has been larger than  $R_{\text{comm}}$  for the past  $T_{\text{passed}} \geq 1$  time steps. This termination condition indicates successful obstacle avoidance.

The obstacle avoidance validation metric is the fraction of terminations not due to passing the obstacle.

Now, we describe our obstacle avoidance technique. At a high level, we have the followers orbit the obstacle, and then we use the leaders to draw the followers away from the obstacle and terminate the followers' orbits. The technique influences the acceleration of a follower  $i$  by formulating the relative velocity  $-\dot{\mathbf{r}}_{ij} = \dot{\mathbf{r}}_{ji}$  between it and an obstacle agent  $j$ . Notice that we wrote the relative velocity vector so that it is rooted at the velocity of the follower  $i$ . This lets us work from the reference frame of the follower.

The technique defines the interaction between a follower agent and a single obstacle agent. As we will later show empirically, all these pairwise interactions culminate in the flock's obstacle-avoidance capability. To implement our technique, we define a parametrized linear discriminant to make two classifications about a follower: (1) whether the follower is moving towards or away from an obstacle agent, and (2) whether the obstacle agent is on the left or right side of the follower's heading. The parameterized linear discriminant is

$$\gamma(\mathbf{r}, \mathbf{v}, \theta) = \frac{\mathbf{r}^\top \mathbf{R}(\theta) \mathbf{v}}{\|\mathbf{r}\| \|\mathbf{v}\|}, \quad (10)$$

for  $\mathbf{r}, \mathbf{v} \neq \mathbf{0}$  and rotation matrix  $\mathbf{R}(\cdot)$ . Fixing  $\hat{\mathbf{x}}_i$ , the linear discriminant  $\mathbf{r}_{ji} \mapsto \gamma(\mathbf{r}_{ji}, \hat{\mathbf{x}}_i, 0)$  classifies whether the follower is moving toward (positive value) or away (negative value) from the obstacle agent. Moreover, the linear discriminant  $\mathbf{r}_{ji} \mapsto \gamma(\mathbf{r}_{ji}, \hat{\mathbf{x}}_i, \frac{\pi}{2})$  classifies whether the obstacle agent is to the left (positive value) or right (negative value) of the follower's heading. These linear discriminants are assembled to determine how the follower should accelerate when receiving the position of an obstacle agent. When the follower accelerates,  $\hat{\mathbf{x}}_i$  changes, and so do the outputs of the linear discriminants. To



reduce the linear discriminants sensitivity to  $\dot{\mathbf{x}}_i$ , we replace  $\dot{\mathbf{x}}_i$  with the mean velocity of the follower and its neighbors:  $\bar{\mathbf{v}}_i(t) = \text{mean}\{\dot{\mathbf{x}}_j(t) : j \in \mathcal{N}_i(t) \cup \{i\}\}$ .

Finally, our technique formulates the relative velocity as

$$-\dot{\mathbf{r}}_{ij}(t) = \begin{cases} \alpha_1(\|\mathbf{r}_{ji}\|, \|\bar{\mathbf{v}}_i\|) \frac{\mathbf{r}_{ji}}{\|\mathbf{r}_{ji}\|} & \text{if } -\alpha_2 \leq \gamma(\mathbf{r}_{ji}, \bar{\mathbf{v}}_i, 0) \leq 0, \\ \alpha_1(\|\mathbf{r}_{ji}\|, \|\bar{\mathbf{v}}_i\|) (-\text{sgn}[\gamma(\mathbf{r}_{ji}, \bar{\mathbf{v}}_i, \frac{\pi}{2})] \mathbf{R}(\alpha_\theta)) \frac{\mathbf{r}_{ji}}{\|\mathbf{r}_{ji}\|} & \text{else,} \end{cases} \quad (11)$$

where  $\alpha_1 : \mathbb{R}_+^2 \rightarrow \mathbb{R}_+$  is a rescaling function,  $\alpha_2 \in [0, 1]$ , and  $\alpha_\theta \in (0, \frac{\pi}{2}]$ . A follower may have multiple obstacle agent neighbors, but we limit the follower to only process the relative velocity computed from the position of the closest obstacle agent.

We explain the relative velocity formulation considering a follower  $i$ , its flock agent neighbors, and the obstacle agent  $j$  that it is closest to. From the definition, when  $\gamma(\mathbf{r}_{ji}, \bar{\mathbf{v}}_i, 0) > 0$ , the follower is roughly heading toward the obstacle agent, so the relative velocity accelerates the follower to the left or right of the obstacle agent (depending on the sign of  $\gamma(\mathbf{r}_{ji}, \bar{\mathbf{v}}_i, \frac{\pi}{2})$ ). When moving left or right, eventually  $\gamma(\mathbf{r}_{ji}, \bar{\mathbf{v}}_i, 0) \in [-\alpha_2, 0]$ , meaning the follower either is heading tangent to a disk of radius  $\|\mathbf{r}_{ji}\|$  centered at the obstacle agent or is heading away from the obstacle agent. In this case, the relative velocity accelerates the follower toward the obstacle agent, initiating an orbit about the obstacle agent. The orbit helps the follower reunite with the followers that moved around the obstacle agent the opposite way. When  $\alpha_2 = 1$ , the relative velocity accelerates the follower toward the obstacle agent even when its flock agent neighbors are moving away from the obstacle agent. The follower can get stuck in the ‘‘gravity’’ of the obstacle agent, so setting  $\alpha_2 \in [0, 1)$  can help the follower terminate its orbit. When  $\gamma(\mathbf{r}_{ji}, \bar{\mathbf{v}}_i, 0) < -\alpha_2$  and  $\alpha_\theta = \pi/2$ , the relative velocity accelerates the followers in the direction tangent to a disk of radius  $\|\mathbf{r}_{ji}\|$  centered at the obstacle agent.

The followers are drawn away from the obstacle agents by the leaders because the leaders will always eventually head away from all of the obstacle agents. The followers try to align their velocity with the leaders’ velocity, and if they can,  $\gamma(\mathbf{r}_{ji}, \bar{\mathbf{v}}_i, 0)$  will become negative. How closely the followers need to align their velocity with the leaders in order to move away from the obstacle agents depends on  $\alpha_2$ . In our experiment, we choose  $\alpha_2 = 0.5$ ,  $\alpha_\theta = \pi/2$ , and  $\alpha_1$  as  $\alpha_1(r, v) = e^{-r} + e^{-v}$ . We offer an intuition for our choice of  $\alpha_1$ . The  $e^{-\|\mathbf{r}_{ji}\|}$  term amplifies the acceleration supplied by the relative velocity when the follower and obstacle agent are closer. The  $e^{-\|\bar{\mathbf{v}}_i\|}$  term strengthens the acceleration if the follower slows down to avoid colliding with the obstacle. This helps the follower maintain the magnitude of its velocity prior to detecting the obstacle, allowing the flock to circumnavigate the obstacle faster. Attenuating the signal when the follower’s velocity is small would allow it to stall in front of the obstacle and fall behind the leaders.

Fig. 8 shows the failure rate of ML controllers on the test simulations when they do *not* use our technique. Their failure rate is near 100% with over 95% of failures due to disconnected communication graphs. Using our obstacle avoidance technique makes obstacle avoidance possible for ML controllers, as

shown in Fig. 9. When the obstacle perimeter is  $24R_{\min}$  or smaller, the failure fraction decreases by at least 80% for all ML controllers. It decreases by 55% for perimeter  $48R_{\min}$  and at least 10% for perimeter  $96R_{\min}$ .

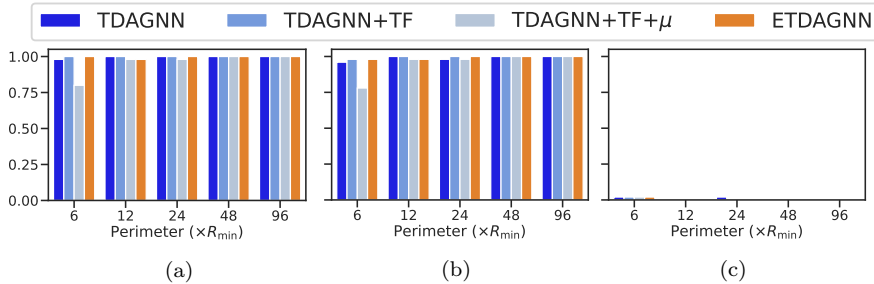


Fig. 8: Performance of ML controllers in obstacle avoidance varying the perimeter of the regular polygon inscribed in the obstacle when our obstacle avoidance technique is *not* used. The obstacle is a disk, and the regular polygon has  $s$  sides of length  $R_{\min}$  whose vertices are on the boundary of the disk. They are evaluated on the RandomDisk test set with  $N = 100$  agents where two agents are leaders. (a) Fraction of simulations that failed. (b) Fraction of failures due to a disconnected communication graph. (c) Fraction of failures due to a collision.

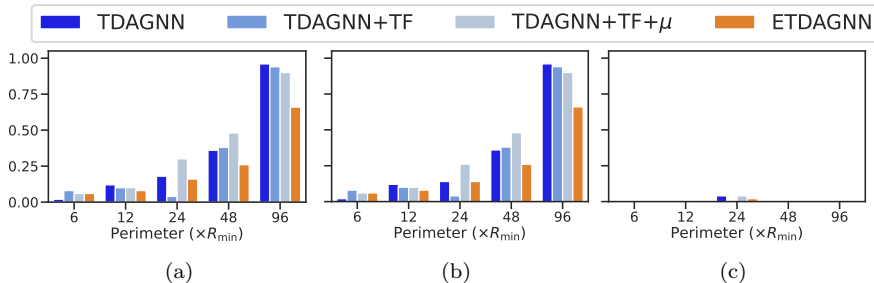


Fig. 9: Performance of ML controllers in obstacle avoidance using our obstacle avoidance technique varying the perimeter of the regular polygon inscribed in the obstacle. The obstacle is a disk, and the regular polygon has  $s$  sides of length  $R_{\min}$  whose vertices are on the boundary of the disk. They are evaluated on the RandomDisk test set with  $N = 100$  agents where two agents are leaders. (a) Fraction of simulations that failed. (b) Fraction of failures due to a disconnected communication graph. (c) Fraction of failures due to a collision.

Communication graph disconnection is still the dominant cause of failure. Failures due to collisions with the obstacle only occur when the obstacle perimeter is  $24R_{\min}$ , representing less than 5% of failures. ETDAGNN has a failure rate at least 10% lower than other controllers when the obstacle perimeter is  $48R_{\min}$ , and 20% lower for perimeter  $96R_{\min}$ . For perimeter  $48R_{\min}$  and  $96R_{\min}$ , the other ML controllers' failure rates are within 10% of each other. For obstacles a perimeter  $6R_{\min}$  or smaller, all ML controllers have a failure rate of less than 10%. For larger obstacles, we recommend ETDAGNN since its failure fraction is up to 20% smaller than other ML controllers. Rotation equivariance provides a significant performance advantage in this obstacle avoidance experiment. Animations of obstacle avoidance are available on GitHub.<sup>4</sup>

#### 6.4 Generalization gap

We verify the generalization bound in Eqn. (8) for each ML controller with respect to its FFBC dataset. Each dataset has 80,400 tuples with 30,150 for training and 50,250 for testing. We train the ML controllers on their training sets with  $C = 2$ , and evaluate them on their test sets. The constant  $C$  helps avoid the loss gradients being zero due to the  $\min\{1, \cdot\}$  function. We compute the generalization bound in Eqn. (8) with  $\delta = 10^{-3}$  and the empirical bound. The empirical generalization bound is the difference of the empirical risk over the test set minus the empirical risk over the training set

$$\hat{\mathcal{R}}_{\mathcal{B}^{\text{test}}, \mathcal{B}, \mathcal{L}}(f) = \frac{1}{B^{\text{test}}} \sum_{b=1}^{B^{\text{test}}} \mathcal{L}(f(x_b^{\text{test}}), y^{\text{test}}) - \frac{1}{B} \sum_{b=1}^B \mathcal{L}(f(x_b), y).$$

Fig. 10 and 11 show that the empirical generalization gap is near zero for all controllers. Here, the training and the test sets are sampled from the same probability distribution induced by FFBC.

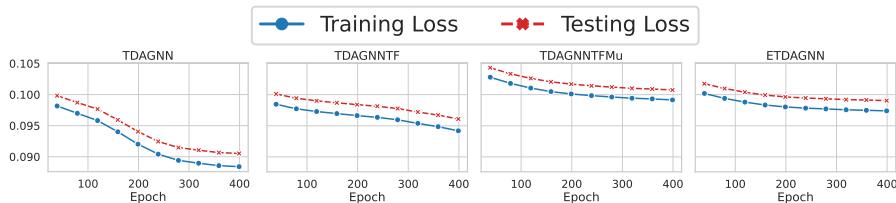


Fig. 10: The losses on the behavior cloning training and test sets as the flocking ML controllers train.

<sup>4</sup> Obstacle avoidance animations: [github.com/Utah-Math-Data-Science/Equivariant-Decentralized-Controllers/tree/main/misc/animations/obstacle\\_avoidance](https://github.com/Utah-Math-Data-Science/Equivariant-Decentralized-Controllers/tree/main/misc/animations/obstacle_avoidance)

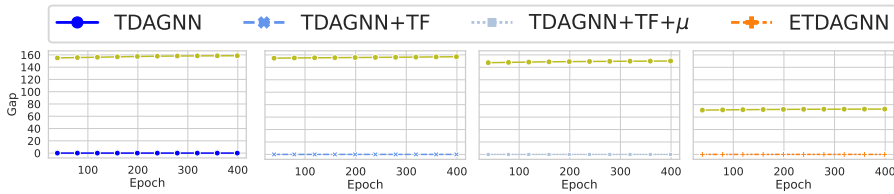


Fig. 11: The generalization bound and empirical generalization gap over epochs. The generalization bound improves with the ML controllers from left to right, and adding equivariance lowers the generalization gap the most.

The generalization bound reduces as we add the improvements (described in section 4.3) to TDAGNN. Enforcing equivariance significantly reduces the generalization gap, as ETDAGNN’s bound is about half that of TDAGNN+TF+ $\mu$ . The term in the generalization bound that varies between ML controllers is  $48d/\sqrt{B}$  multiplied by the square root term  $\sqrt{\cdot}$ . Fig. 12 gives insight into how these terms influence the generalization bound. The plot of  $48d/\sqrt{B}$  explains why the generalization bound of ETDAGNN is about half of the non-equivariant controllers’ – ETDAGNN has  $d = 16$  whereas the non-equivariant ML controllers have  $d = 33$ . Next,  $\beta$  is an order of magnitude smaller for mean-aggregation controllers compared to sum-aggregation; however, it only introduces a 10-point difference between the bounds of TDAGNN+TF and TDAGNN+TF+ $\mu$  seen in the square root term  $\sqrt{\cdot}$ . The summation depending on the Frobenius norm of the weight matrices is remarkably similar for the non-equivariant controllers and ETDAGNN. ETDAGNN has about 75% fewer weights (see Table 2), so its weights tend to be larger than that of the non-equivariant controllers. Though these bounds are much larger than the empirical generalization gap, Fig. 13 shows that they have a high correlation ( $\rho \geq 0.95$ ) with the empirical generalization gap.

## 7 Conclusion

In response to the challenges in building decentralized flocking controllers, we presented an enhanced ML-based decentralized flocking controller that leverages a rotation equivariant and translation invariant GNN. We demonstrated the advantages of the proposed decentralized controller over existing non-equivariant ML-based controllers and other flocking controllers using three representative case studies – flocking, leader following, and obstacle avoidance. We also analyzed the generalization gap of the proposed decentralized flocking controller. Our numerical results show that the proposed decentralized controller achieves comparable performance compared to non-equivariant ML-based controllers with 70% less training data, 75% fewer trainable weights and a 50% smaller generalization bound.

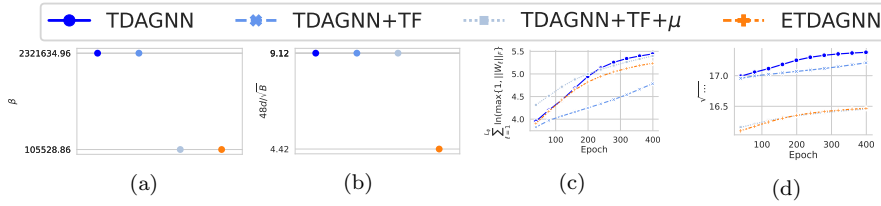


Fig. 12: Select terms of the generalization bound for each ML controller as it trains on its FFBC dataset. (a) The FFBC data bound. (b) The coefficient to the large square root term in the generalization bound. These terms are constant with respect to epochs. The data bound of TDAGNN+TF+ $\mu$  and ETDAGNN (mean-aggregation ML controllers) is an order of magnitude smaller compared to TDAGNN and TDAGNN+TF (sum-aggregation ML controllers). The coefficient term of ETDAGNN is less than half that of the other ML controllers. The terms in the generalization gap bound that depend on the Frobenius norm of the ML controllers’ weight matrices when represented as MLPs are (c) the summation and (d) the large square root term containing that summation.

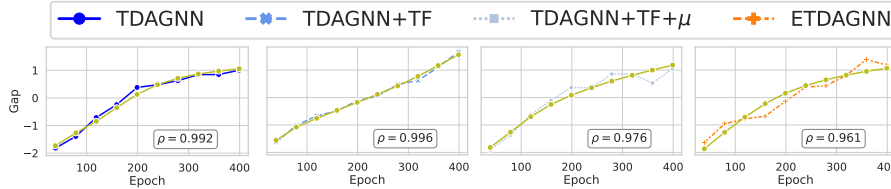


Fig. 13: The correlation of generalization bound and empirical generalization gap. We plot each of these sequences over epochs with their mean subtracted and divided by their standard deviation.

## Declarations

Data availability

Code and animations are available at [github.com/Utah-Math-Data-Science/Equivariant-Decentralized-Controllers](https://github.com/Utah-Math-Data-Science/Equivariant-Decentralized-Controllers).

## Funding

This material is based on research sponsored by National Science Foundation (NSF) grants DMS-2152762, DMS-2208361, DMS-2219956, and DMS-2436344, and Department of Energy grants DE-SC0023490, DE-SC0025589, and DE-SC0025801. Taos Transue received partial financial support from the NSF under Award 2136198.

## Competing interests

All authors certify that they have no affiliations with or involvement in any organization or entity with any financial interest or non-financial interest in the subject matter or materials discussed in this manuscript.

## A Proofs

### A.1 Preliminaries

**Lemma 2 (Frobenius norm upper bounds spectral norm)** *Let  $\mathbf{A} \in \mathbb{R}^{m \times n}$ , and then  $\|\mathbf{A}\|_2 \leq \|\mathbf{A}\|_F$ .*

*Proof* Let  $\mathbf{A} = \mathbf{U}\mathbf{\Sigma}\mathbf{V}^\top$  be the singular value decomposition of  $\mathbf{A}$  where  $\mathbf{U} \in \mathbb{R}^{m \times m}$  and  $\mathbf{V} \in \mathbb{R}^{n \times n}$  are orthogonal matrices. Let  $\sigma_i$  and  $\sigma_{\max}$  denote the  $i$ -th and the largest singular value, respectively. Then,

$$\|\mathbf{A}\|_2 = \|\mathbf{U}\mathbf{\Sigma}\mathbf{V}^\top\|_2 = \|\mathbf{\Sigma}\|_2 = \sigma_{\max} \leq \sum_{i=1}^{\min\{m,n\}} \sigma_i = \|\mathbf{\Sigma}\|_F = \|\mathbf{U}\mathbf{\Sigma}\mathbf{V}^\top\|_F = \|\mathbf{A}\|_F$$

This bound is sharp since, for  $c \in \mathbb{R}^{1 \times 1}$ ,  $\|c\|_2 = |c| = \|c\|_F$ .

### A.2 Generalization gap

**Lemma 3** *Let  $\phi$  be either TDAGNN, TDAGNN+TF, or TDAGNN+TF+ $\mu$ . Then,*

$$\|\phi(\mathbf{H}_{i,1})\| = \|\Phi(\mathbf{H}_{i,1}^{\text{MLP}})\| \leq \left(\prod_{\ell=1}^{L_\phi} K_\sigma \|\mathbf{W}_\ell\|_F\right) \|\mathbf{H}_{i,1}^{\text{MLP}}\|_F,$$

where  $\Phi$  is the MLP representation of  $\phi$ ,  $\mathbf{H}_{i,1}^{\text{MLP}}$  is from Definition 6,  $K_\sigma \geq 1$  bounds the largest Lipschitz constant of the activations used by  $\phi$ , and  $\{\mathbf{W}_\ell\}_{\ell=1}^{L_\phi}$  are the weight matrices of  $\Phi$ .

*Proof* The activations of  $\phi$  are either  $\sigma_\ell(x) = \tanh(x)$  or  $\sigma_\ell(x) = x$  for  $\ell \in \{1, \dots, L_\phi\}$ . Both have Lipschitz constant  $K_\sigma = 1$  and satisfy  $\sigma(0) = 0$ . By lemma 8,  $\phi$  can be expressed as an MLP  $\Phi$ . Adapting Lemma B.1 of [18],

$$\begin{aligned} \|\Phi_{L_\phi}(\mathbf{H}_{i,1}^{\text{MLP}})\|_2 &= \|\sigma_{L_\phi}(\Phi_{L_\phi-1}(\mathbf{H}_{i,1}^{\text{MLP}})\mathbf{W}_{L_\phi})\|_2 = \|\sigma_{L_\phi}(\Phi_{L_\phi-1}(\mathbf{H}_{i,1}^{\text{MLP}})\mathbf{W}_{L_\phi}) - \sigma_{L_\phi}(\mathbf{0})\|_2 \\ &\leq K_\sigma \|\Phi_{L_\phi-1}(\mathbf{H}_{i,1}^{\text{MLP}})\mathbf{W}_{L_\phi}\|_2 \leq K_\sigma \|\mathbf{W}_{L_\phi}\|_2 \|\Phi_{L_\phi-1}(\mathbf{H}_{i,1}^{\text{MLP}})\|_2 \\ &\leq \dots \leq \left(\prod_{\ell=1}^{L_\phi} K_\sigma \|\mathbf{W}_\ell\|_2\right) \|\mathbf{H}_{i,1}^{\text{MLP}}\|_2 \\ &= \left(\prod_{\ell=1}^{L_\phi} K_\sigma \|\mathbf{W}_\ell\|_2\right) \|\mathbf{H}_{i,1}^{\text{MLP}}\|_F \quad \text{by Definition 6} \\ &\leq \left(\prod_{\ell=1}^{L_\phi} K_\sigma \|\mathbf{W}_\ell\|_F\right) \|\mathbf{H}_{i,1}^{\text{MLP}}\|_F \quad \text{by Lemma 2} \end{aligned}$$

**Lemma 4** Let  $\phi$  be an ETDAGNN. Then,

$$\|\phi(\mathbf{H}_{i,1})\| = \|\Phi(\mathbf{H}_{i,1}^{\text{MLP}})\| \leq \left(\prod_{\ell=1}^{L_\phi} K_\sigma \|\mathbf{W}_\ell\|_F\right) \|\mathbf{H}_{i,1}^{\text{MLP}}\|_F,$$

where  $\Phi$  is the MLP representation of ETDAGNN,  $\mathbf{H}_{i,1}^{\text{MLP}}$  is defined in Definition 7,  $K_\sigma \geq 1$  bounds the largest Lipschitz constant of the activations in ETDAGNN, and  $\{\mathbf{W}_\ell\}_{\ell=1}^{L_\phi}$  are the weight matrices of  $\Phi$ .

*Proof*  $\phi$  uses the  $O(n)$  equivariant activations  $\sigma_\ell \in \{\sigma_{\text{in}}, \sigma_{\text{tanh}}, \mathbf{x} \mapsto \mathbf{x}\}$  for  $\ell \in \{1, \dots, L_\phi\}$ . Let  $K_\sigma$  be the maximum of their Lipschitz constants. By Lemma 13, 14, and 15,  $\sigma_\ell$  is an  $O(2)$  equivariant activation with global Lipschitz  $K_\sigma$  in the Frobenius norm, and  $\sigma_\ell(\mathbf{0}) = \mathbf{0}$  by Lemma 10. Next, by Lemma 9,  $\phi$  can be expressed as an MLP  $\Phi$ . Adapting Lemma B.1 of [18],

$$\begin{aligned} \|\Phi_{L_\phi}(\mathbf{H}_{i,1}^{\text{MLP}})\|_2 &= \|\sigma_{L_\phi}(\Phi_{L_\phi-1}(\mathbf{H}_{i,1}^{\text{MLP}})\mathbf{W}_{L_\phi})\|_2 = \|\sigma_{L_\phi}(\Phi_{L_\phi-1}(\mathbf{H}_{i,1}^{\text{MLP}})\mathbf{W}_{L_\phi}) - \sigma_{L_\phi}(\mathbf{0})\|_2 \\ &\leq K_\sigma \|\Phi_{L_\phi-1}(\mathbf{H}_{i,1}^{\text{MLP}})\mathbf{W}_{L_\phi}\|_2 \leq K_\sigma \|\mathbf{W}_{L_\phi}\|_2 \|\Phi_{L_\phi-1}(\mathbf{H}_{i,1}^{\text{MLP}})\|_2 \\ &\leq \dots \leq \left(\prod_{\ell=1}^{L_\phi} K_\sigma \|\mathbf{W}_\ell\|_2\right) \|\mathbf{H}_{i,1}^{\text{MLP}}\|_2 \\ &\leq \left(\prod_{\ell=1}^{L_\phi} K_\sigma \|\mathbf{W}_\ell\|_F\right) \|\mathbf{H}_{i,1}^{\text{MLP}}\|_F \quad \text{by Lemma 2} \end{aligned}$$

**Lemma 5** Let the scoring model  $h_{\mathcal{G}}$  be as given in Eqn. (7) equivalently written to take an FFBC tuple as input. Using assumption 4,

$$h_{\mathcal{G}}(\mathbf{X}, \dot{\mathbf{X}}, \{\mathbf{H}_i\}_{i=1}^N) \leq w^2 + \left(1 + \left(\prod_{\ell=1}^{L_\phi} K_\sigma \|\mathbf{W}_\ell\|_F\right)^2\right) \beta^2.$$

*Proof* Using Assumption 4, and Lemma 3 and 4,

$$\begin{aligned} h_{\mathcal{G}}(\mathbf{X}, \dot{\mathbf{X}}, \{\mathbf{H}_i\}_{i=1}^N) &\leq w^2 + \frac{1}{N} \sum_{i=1}^N \|\mathbf{a}_i(\mathbf{X}, \dot{\mathbf{X}})\|^2 + \|\phi(\mathbf{H}_{i,1})\|^2 \\ &= w^2 + \frac{1}{N} \sum_{i=1}^N \|\mathbf{a}_i(\mathbf{X}, \dot{\mathbf{X}})\|^2 + \|\Phi(\mathbf{H}_{i,1}^{\text{MLP}})\|^2 \\ &\leq w^2 + \frac{1}{N} \sum_{i=1}^N \|\mathbf{a}_i(\mathbf{X}, \dot{\mathbf{X}})\|_F^2 + \left(\prod_{\ell=1}^{L_\phi} K_\sigma \|\mathbf{W}_\ell\|_F\right)^2 \|\mathbf{H}_{i,1}^{\text{MLP}}\|_F^2 \\ &\leq w^2 + \frac{1}{N} \sum_{i=1}^N \beta^2 + \left(\prod_{\ell=1}^{L_\phi} K_\sigma \|\mathbf{W}_\ell\|_F\right)^2 \beta^2 \\ &\leq w^2 + \left(1 + \left(\prod_{\ell=1}^{L_\phi} K_\sigma \|\mathbf{W}_\ell\|_F\right)^2\right) \beta^2. \end{aligned}$$

The ML controllers are parameterized by weight matrices, which have a bounded covering number (Lemma 8 of [6]). Using Lemma G.1 of [18], if we can show the ML controllers are Lipschitz with respect to the weight matrices, then we can bound the covering number of the ML controllers. Next, we show that the ML controllers and their scoring function are Lipschitz.

**Lemma 6 (Lipshitz continuity of TDAGNN)** Let  $\phi$  be either TDAGNN, TDAGNN+TF, TDAGNN+TF+ $\mu$ , or ETDAGNN with an MLP representation  $\Phi$ . Take two functions  $\Phi(\mathbf{H}_{i,1}^{\text{MLP}}; \mathcal{W})$  and  $\Phi(\mathbf{H}_{i,1}^{\text{MLP}}; \tilde{\mathcal{W}})$  with  $L_\phi$  layers where  $\mathcal{W}$  and  $\tilde{\mathcal{W}}$  are collections of weight matrices. Let  $\beta_\ell \geq 1$  s.t.  $\max\{\|\mathbf{W}_\ell\|_F, \|\tilde{\mathbf{W}}_\ell\|_F\} \leq \beta_\ell$ . Then,

$$\|\Phi(\mathbf{H}_{i,1}^{\text{MLP}}; \mathcal{W}) - \Phi(\mathbf{H}_{i,1}^{\text{MLP}}; \tilde{\mathcal{W}})\| \leq \|\mathbf{H}_{i,1}^{\text{MLP}}\|_F \left( \prod_{\ell=1}^{L_\phi} K_\sigma \beta_\ell \right) \sum_{\ell=1}^{L_\phi} \|\mathbf{W}_\ell - \tilde{\mathbf{W}}_\ell\|_F,$$

where  $K_\sigma \geq 1$  bounds the largest Lipshitz constant of the activations used by  $\Phi$ .

*Proof* The proof follows the proof of Lemma B.2 of [18] where  $\|\cdot\| = \|\cdot\|_F$ .

**Lemma 7** Let  $\Phi$  be the MLP representation of  $\phi$  and  $h_{\mathcal{G}}$  be as defined in Eqn. (7). Consider two parameterizations of  $\Phi$  and  $h_{\mathcal{G}}$ :  $\{w, \mathcal{W}\}, \{\tilde{w}, \tilde{\mathcal{W}}\}$ . Let  $\beta_\ell \geq 1$  and  $\beta_{h_{\mathcal{G}}} \geq 1$  where  $\max\{\|\mathbf{W}_\ell\|_F, \|\tilde{\mathbf{W}}_\ell\|_F\} \leq \beta_\ell$  and  $\max\{|w|, |\tilde{w}|\} \leq \beta_{h_{\mathcal{G}}}$ . By Assumption 4,

$$\begin{aligned} & |h_{\mathcal{G}}(\mathbf{X}, \dot{\mathbf{X}}, \{\mathbf{H}_i\}_{i=1}^N; \mathcal{W}, w) - h_{\mathcal{G}}(\mathbf{X}, \dot{\mathbf{X}}, \{\mathbf{H}_i\}_{i=1}^N; \tilde{\mathcal{W}}, \tilde{w})| \\ & \leq 2\beta_{h_{\mathcal{G}}} |w - \tilde{w}| + 2(1 + \Psi)\beta^2 \Psi \sum_{\ell=1}^{L_\phi} \|\mathbf{W}_\ell - \tilde{\mathbf{W}}_\ell\|_F. \end{aligned}$$

where  $\Psi = \prod_{\ell=1}^{L_\phi} K_\sigma \beta_\ell$ .

*Proof*

$$\begin{aligned} & |h_{\mathcal{G}}(\cdot; \mathcal{W}) - h_{\mathcal{G}}(\cdot; \tilde{\mathcal{W}})| \\ & = |w^2 + \frac{1}{N} \sum_{i=1}^N \|\mathbf{a}_i(\mathbf{X}, \dot{\mathbf{X}}) - \Phi(\mathbf{H}_{i,1}^{\text{MLP}}; \mathcal{W})\|^2 - w^2 - \frac{1}{N} \sum_{i=1}^N \|\mathbf{a}_i(\mathbf{X}, \dot{\mathbf{X}}) - \Phi(\mathbf{H}_{i,1}^{\text{MLP}}; \tilde{\mathcal{W}})\|^2| \\ & \leq |w^2 - \tilde{w}^2| + \frac{1}{N} \sum_{i=1}^N \|\|\mathbf{a}_i(\mathbf{X}, \dot{\mathbf{X}}) - \Phi(\mathbf{H}_{i,1}^{\text{MLP}}; \mathcal{W})\|^2 - \|\mathbf{a}_i(\mathbf{X}, \dot{\mathbf{X}}) - \Phi(\mathbf{H}_{i,1}^{\text{MLP}}; \tilde{\mathcal{W}})\|^2|. \end{aligned}$$

Using the fact  $\|\|\mathbf{x} - \mathbf{a}\|^2 - \|\mathbf{x} - \mathbf{b}\|^2\| \leq (2\|\mathbf{x}\| + \|\mathbf{a}\| + \|\mathbf{b}\|)\|\mathbf{a} - \mathbf{b}\|$ ,  $\|\mathbf{a}_i(\mathbf{X}, \dot{\mathbf{X}})\| \leq \beta$  by Assumption 4, and  $\|\Phi(\mathbf{H}_{i,1}^{\text{MLP}})\| \leq (\prod_{\ell=1}^{L_\phi} K_\sigma \|\mathbf{W}_\ell\|_F) \|\mathbf{H}_{i,1}^{\text{MLP}}\|_F \leq \Psi \|\mathbf{H}_{i,1}^{\text{MLP}}\|_F$  by Lemma 3 or 4,

$$|h_{\mathcal{G}}(\cdot; \mathcal{W}) - h_{\mathcal{G}}(\cdot; \tilde{\mathcal{W}})| \leq 2\beta_{h_{\mathcal{G}}} |w - \tilde{w}| + \frac{2}{N} \sum_{i=1}^N (\beta + \Psi \|\mathbf{H}_{i,1}^{\text{MLP}}\|_F) \|\Phi(\mathbf{H}_{i,1}^{\text{MLP}}; \mathcal{W}) - \Phi(\mathbf{H}_{i,1}^{\text{MLP}}; \tilde{\mathcal{W}})\|.$$

By Lemma 6,

$$\begin{aligned} & |h_{\mathcal{G}}(\cdot; \mathcal{W}) - h_{\mathcal{G}}(\cdot; \tilde{\mathcal{W}})| \\ & \leq 2\beta_{h_{\mathcal{G}}} |w - \tilde{w}| + \frac{2}{N} \sum_{i=1}^N (\beta + \Psi \|\mathbf{H}_{i,1}^{\text{MLP}}\|_F) \|\mathbf{H}_{i,1}^{\text{MLP}}\|_F \Psi \sum_{\ell=1}^{L_\phi} \|\mathbf{W}_\ell - \tilde{\mathbf{W}}_\ell\|_F. \end{aligned}$$

Using that  $\|\mathbf{H}_{i,1}^{\text{MLP}}\|_F \leq \beta$  by Assumption 4,

$$\begin{aligned} |h_{\mathcal{G}}(\cdot; \mathcal{W}) - h_{\mathcal{G}}(\cdot; \tilde{\mathcal{W}})| & \leq 2\beta_{h_{\mathcal{G}}} |w - \tilde{w}| + \frac{2}{N} \sum_{i=1}^N (\beta + \Psi\beta) \Psi \sum_{\ell=1}^{L_\phi} \|\mathbf{W}_\ell - \tilde{\mathbf{W}}_\ell\|_F \\ & = 2\beta_{h_{\mathcal{G}}} |w - \tilde{w}| + 2(1 + \Psi)\beta^2 \Psi \sum_{\ell=1}^{L_\phi} \|\mathbf{W}_\ell - \tilde{\mathbf{W}}_\ell\|_F. \end{aligned}$$



With the above supporting lemmas, we are ready to prove the following result:

**Proposition 2 (Generalization bound of TDAGNN)** *Let  $P$  be the probability distribution over tuples  $(\mathbf{X}, \dot{\mathbf{X}}, \{\mathbf{H}_i\}_{i=1}^N)$  induced by FFBC. Let  $\mathcal{L}(y) = \min\{1, y/C\}$  for  $C > 0$  be the loss function. Let  $\{\mathbf{W}_\ell\}_{\ell=1}^{L_\phi}$  be the weights of the MLP representation  $\Phi$  of  $\phi$  given by Lemma 8 or 9, and let  $w$  of  $h_G$  in Eqn. (7) such that  $w \in [0, \sqrt{C}]$ . For any  $\delta > 0$ , with probability at least  $1 - \delta$  over choosing a batch  $\mathcal{B}$  of  $B$  tuples sampled from  $P$ , the following bound holds:*

$$\begin{aligned} \mathcal{R}_{\mathcal{B}, \mathcal{L}}(h_G) &\leq \frac{8}{B} \\ &+ \frac{48d}{\sqrt{B}} \sqrt{(3L_\phi + 1) \ln(10L_\phi \beta K_\sigma^{L_\phi} \sqrt{dBC}) + (2L_\phi + 3) \sum_{\ell=1}^{L_\phi} \ln(\max\{1, \|\mathbf{W}_\ell\|_F\})} + 3\sqrt{\frac{\ln(\frac{2}{\delta})}{2B}}. \end{aligned}$$

*Proof* Let  $\mathcal{F} = \{h_G(\cdot; \mathcal{W}, w) : \mathcal{W} = \{\mathbf{W}_\ell\}_{\ell=1}^{L_\phi}, \|\mathbf{W}_\ell\|_F \leq \beta_\ell, |w| \leq \beta_{h_G}\}$ , where  $\beta_{h_G} = \sqrt{C}$ . Define the set of datum-to-loss functions  $\mathcal{F}_\mathcal{L} = \{(\mathbf{X}, \dot{\mathbf{X}}, \{\mathbf{H}_i\}_{i=1}^N) \mapsto \mathcal{L}(h_G(\mathbf{X}, \dot{\mathbf{X}}, \{\mathbf{H}_i\}_{i=1}^N)) : h_G \in \mathcal{F}\}$ . We follow the steps from proof of Proposition 4.1 from [18]. Applying these steps requires that we find an  $\hat{f}_0 \in \hat{\mathcal{F}}_\mathcal{L}$  where

$$\hat{\mathcal{F}}_\mathcal{L} = \{(\mathbf{X}, \dot{\mathbf{X}}, \{\mathbf{H}_i\}_{i=1}^N) \mapsto 1 - \mathcal{L}(h_G(\mathbf{X}, \dot{\mathbf{X}}, \{\mathbf{H}_i\}_{i=1}^N)) : h_G \in \mathcal{F}\},$$

and  $\hat{f}_0(\mathbf{X}, \dot{\mathbf{X}}, \{\mathbf{H}_i\}_{i=1}^N) = 0$  for all  $(\mathbf{X}, \dot{\mathbf{X}}, \{\mathbf{H}_i\}_{i=1}^N)$  satisfying Assumption 4. By definition of  $\mathcal{L}$ , we can construct  $\hat{f}_0$  by finding  $h_G$  s.t.  $h_G(\mathbf{X}, \dot{\mathbf{X}}, \{\mathbf{H}_i\}_{i=1}^N) \geq C$  for all  $(\mathbf{X}, \dot{\mathbf{X}}, \{\mathbf{H}_i\}_{i=1}^N)$ . This can be achieved by setting the kernel weights and bias weights (if present) of  $\phi$  to zero, and setting  $w$  of  $h_G$  in Eqn. (7) to  $w = \sqrt{C}$ . Therefore, we choose  $\hat{f}_0(\cdot) = 1 - \mathcal{L}(h_G(\cdot; \{\mathbf{0}\}_{\ell=1}^{L_\phi}, \sqrt{C}))$ . With  $\hat{f}_0$  found, we follow [18] to obtain

$$\hat{\mathfrak{H}}_\mathcal{B}(\mathcal{F}_\mathcal{L}) \leq \frac{4}{B} + \frac{24}{B} \sqrt{\ln \mathcal{N}(\mathcal{F}, \frac{1}{2\sqrt{B}}, \|\cdot\|_F)}.$$

Next, we adapt the steps in [18] to bound  $\ln \mathcal{N}(\mathcal{F}, \frac{1}{2\sqrt{B}}, \|\cdot\|_\infty)$ . Using Lemma 7, we bound the supremum distance between functions in  $\mathcal{F}$  by a function of the distance between their weight matrices:

$$\begin{aligned} &\|h_G(\cdot; \mathcal{W}, w) - h_G(\cdot; \tilde{\mathcal{W}}, \tilde{w})\|_\infty \\ &= \sup_{(\mathbf{X}, \dot{\mathbf{X}}, \{\mathbf{H}_i\}_{i=1}^N) \in \mathcal{D}} |h_G(\mathbf{X}, \dot{\mathbf{X}}, \{\mathbf{H}_i\}_{i=1}^N; \mathcal{W}) - h_G(\mathbf{X}, \dot{\mathbf{X}}, \{\mathbf{H}_i\}_{i=1}^N; \tilde{\mathcal{W}})| \\ &\leq 2\beta_{h_G} |w - \tilde{w}| + 2(1 + \Psi)\beta^2 \Psi \sum_{\ell=1}^{L_\phi} \|\mathbf{W}_\ell - \tilde{\mathbf{W}}_\ell\|_F \\ &\leq \underbrace{2(\beta_{h_G} + (1 + \Psi)\beta^2 \Psi)}_{:=K_{h_G}} (|w - \tilde{w}| + \sum_{\ell=1}^{L_\phi} \|\mathbf{W}_\ell - \tilde{\mathbf{W}}_\ell\|_F). \end{aligned}$$

Using that bound, Lemma G.1 from [18] bounds the covering number of  $\mathcal{F}$  by the covering number of the weight matrices.

$$\ln \mathcal{N}(\mathcal{F}, r, \|\cdot\|_\infty) \leq \ln \mathcal{N}(w \in [0, \sqrt{C}], \frac{r}{L_\phi K_{h_G}}, |\cdot|) + \sum_{\ell=1}^{L_\phi} \ln \mathcal{N}(\mathcal{W}_\ell, \frac{r}{L_\phi K_{h_G}}, \|\cdot\|_F),$$

where  $\mathcal{W}_\ell$  is the set of possible matrices for  $\mathbf{W}_\ell$ . Using Lemma 3.2 from [6],

$$\ln \mathcal{N}(\mathcal{W}_\ell, \frac{r}{L_\phi K_{h_G}}, \|\cdot\|_F) \leq d^2 \ln(1 + 2 \frac{L_\phi K_{h_G} \beta_\ell \sqrt{d}}{r}),$$

where  $d = \max_{\ell} \dim(\mathbf{W}_{\ell})$ . Choosing  $r = \frac{1}{2\sqrt{B}}$ ,

$$\begin{aligned} \ln \mathcal{N}(\mathcal{F}, \frac{1}{2\sqrt{B}}, \|\cdot\|_{\infty}) &\leq \ln(1 + 4L_{\phi}K_{h_{\mathcal{G}}}\beta_{h_{\mathcal{G}}}\sqrt{B}) + d^2 \sum_{\ell=1}^{L_{\phi}} \ln(1 + 4L_{\phi}K_{h_{\mathcal{G}}}\beta_{\ell}\sqrt{dB}) \\ &\leq \ln(5L_{\phi}K_{h_{\mathcal{G}}}\beta_{h_{\mathcal{G}}}\sqrt{B}) + d^2 \sum_{\ell=1}^{L_{\phi}} \ln(5L_{\phi}K_{h_{\mathcal{G}}}\beta_{\ell}\sqrt{dB}) \\ &\leq d^2 \ln(5L_{\phi}K_{h_{\mathcal{G}}}\beta_{h_{\mathcal{G}}}\sqrt{B}) + d^2 \sum_{\ell=1}^{L_{\phi}} \ln(5L_{\phi}K_{h_{\mathcal{G}}}\beta_{\ell}\sqrt{dB}). \end{aligned}$$

Plugging into the bound for empirical Rademacher complexity,

$$\hat{\mathfrak{R}}_{\mathcal{B}}(\mathcal{F}_{\mathcal{L}}) \leq \frac{4}{B} + \frac{24d}{\sqrt{B}} \sqrt{\underbrace{\ln(5L_{\phi}K_{h_{\mathcal{G}}}\beta_{h_{\mathcal{G}}}\sqrt{B}) + \sum_{\ell=1}^{L_{\phi}} \ln(5L_{\phi}K_{h_{\mathcal{G}}}\beta_{\ell}\sqrt{dB})}_{:=\Sigma}}.$$

Next, we simplify the bound. Using logarithm identities,

$$\Sigma = \frac{L_{\phi}}{2} \ln(d) + (L_{\phi} + 1)[\ln(5L_{\phi}\sqrt{B}) + \ln(K_{h_{\mathcal{G}}})] + \ln(\beta_{h_{\mathcal{G}}}) + \sum_{\ell=1}^{L_{\phi}} \ln(\beta_{\ell}).$$

Finding an upper bound for  $\ln(K_{h_{\mathcal{G}}})$ ,

$$\begin{aligned} \ln(K_{h_{\mathcal{G}}}) &= \ln(2) + \ln(\beta_{h_{\mathcal{G}}} + (1 + \Psi)\beta^2\Psi) \\ &\leq \ln(2) + \ln(\beta_{h_{\mathcal{G}}} + \beta_{h_{\mathcal{G}}}(1 + \Psi)\beta^2\Psi) \\ &\leq \ln(2) + \ln(\beta_{h_{\mathcal{G}}}) + \ln(2(1 + \Psi)\beta^2\Psi) \\ &= 2\ln(2) + \ln(\beta_{h_{\mathcal{G}}}) + \ln(1 + \Psi) + 2\ln(\beta) + \ln(\Psi) \\ &\leq 2\ln(2) + \ln(\beta_{h_{\mathcal{G}}}) + \ln(2\Psi) + 2\ln(\beta) + \ln(\Psi) \\ &= 3\ln(2) + \ln(\beta_{h_{\mathcal{G}}}) + 2\ln(\Psi) + 2\ln(\beta) \\ &= 3\ln(2) + \ln(\beta_{h_{\mathcal{G}}}) + 2\ln\left(\prod_{\ell=1}^{L_{\phi}} K_{\sigma}\beta_{\ell}\right) + 2\ln(\beta) \\ &= 3\ln(2) + \ln(\beta_{h_{\mathcal{G}}}) + 2\ln(\beta) + 2\ln(K_{\sigma}^{L_{\phi}}) + 2\sum_{\ell=1}^{L_{\phi}} \ln(\beta_{\ell}). \end{aligned}$$

Combining these expressions, we find an upper bound for  $\Sigma$ :

$$\begin{aligned} \Sigma &\leq \frac{L_{\phi}}{2} \ln(d) + (L_{\phi} + 1)[\ln(5L_{\phi}\sqrt{B}) + 3\ln(2) + 2\ln(\beta) + 2\ln(K_{\sigma}^{L_{\phi}})] + \\ &\quad (L_{\phi} + 2)\ln(\beta_{h_{\mathcal{G}}}) + (2L_{\phi} + 3)\sum_{\ell=1}^{L_{\phi}} \ln(\beta_{\ell}) \\ &\leq \frac{L_{\phi}}{2} \ln(d) + 3(L_{\phi} + 1)[\ln(5L_{\phi}\sqrt{B}) + \ln(2) + \ln(\beta) + \ln(K_{\sigma}^{L_{\phi}})] + \\ &\quad (L_{\phi} + 2)\ln(\beta_{h_{\mathcal{G}}}) + (2L_{\phi} + 3)\sum_{\ell=1}^{L_{\phi}} \ln(\beta_{\ell}) \\ &\leq 3(L_{\phi} + 1)\ln(10L_{\phi}\beta K_{\sigma}^{L_{\phi}}\beta_{h_{\mathcal{G}}}\sqrt{dB}) + (2L_{\phi} + 3)\sum_{\ell=1}^{L_{\phi}} \ln(\beta_{\ell}). \end{aligned}$$

Using that  $\beta_{h_G} = \sqrt{C}$ ,  $\beta_\ell \leq \max\{1, \|\mathbf{W}_\ell\|_F\}$ , and Theorem 3, we attain the bound for  $\mathcal{R}_{\mathcal{B}, \mathcal{L}}(h_G)$ .

### A.2.1 Convolutional layers as linear layers

**Lemma 8 (Conv1d $_\ell$  as a linear layer)** *Assume that all input channels to Conv1d $_\ell$  :  $\mathbb{R}^{C_\ell \times F_\ell} \rightarrow \mathbb{R}^{C_{\ell+1} \times F_{\ell+1}}$  are of length  $F_\ell$ , then Conv1d $_\ell$  is expressible as a matrix multiplication with a fixed-dimension weight matrix.*

*Proof* Conv1d $_\ell$  :  $\mathbb{R}^{C_\ell \times F_\ell} \rightarrow \mathbb{R}^{C_{\ell+1} \times F_{\ell+1}}$  has  $C_\ell$  input channels that are row vectors of the form

$$\mathbf{H}_{i,\ell}[c_{\text{in}}] = [(\mathbf{H}_{i,\ell})_{c_{\text{in}},1}, \dots, (\mathbf{H}_{i,\ell})_{c_{\text{in}},F_\ell}].$$

Arranging each input channel row vector end to end and appending  $\mathbf{1}_{F_{\ell+1}}^\top$  to account for the bias term, an output channel  $c_{\text{out}} \in \{1, \dots, C_{\ell+1}\}$  is the row vector

$$\mathbf{H}_{i,\ell+1}[c_{\text{out}}] = \text{Conv1d}_\ell(\mathbf{H}_{i,\ell})[c_{\text{out}}] = [\mathbf{H}_{i,\ell}[1], \dots, \mathbf{H}_{i,\ell}[C_\ell], \mathbf{1}_{F_{\ell+1}}^\top] \begin{bmatrix} \mathbf{W}(1, c_{\text{out}}) \\ \vdots \\ \mathbf{W}(C_\ell, c_{\text{out}}) \\ w_{\text{bias}}(c_{\text{out}}) \end{bmatrix}.$$

If  $\ell < L_\phi$ , then all of the output channels may be computed with one matrix multiplication by

$$\begin{aligned} & [\mathbf{H}_{i,\ell}[1], \dots, \mathbf{H}_{i,\ell}[C_\ell], \mathbf{1}_{F_{\ell+1}}^\top] \begin{bmatrix} \mathbf{W}(1,1) & \dots & \mathbf{W}(1,C_{\ell+1}) & \mathbf{0} \\ \vdots & \ddots & \vdots & \\ \mathbf{W}(C_\ell,1) & \dots & \mathbf{W}(C_\ell,C_{\ell+1}) & \mathbf{0} \\ w_{\text{bias}}(1)\mathbf{I} & \dots & w_{\text{bias}}(C_{\ell+1})\mathbf{I} & \mathbf{M} \end{bmatrix} \\ &= [\text{Conv1d}_\ell(\mathbf{H}_{i,\ell})[1], \dots, \text{Conv1d}_\ell(\mathbf{H}_{i,\ell})[C_{\ell+1}], \mathbf{1}_{F_{\ell+2}}^\top], \end{aligned}$$

where  $\mathbf{M} \in \mathbb{R}^{F_{\ell+1} \times F_{\ell+2}}$  maps  $\mathbf{1}_{F_{\ell+1}}^\top$  to  $\mathbf{1}_{F_{\ell+2}}^\top$ . If  $F_{\ell+1} = F_{\ell+2}$ , then  $\mathbf{M} = \mathbf{I}_{F_{\ell+1} \times F_{\ell+1}}$ . If  $F_{\ell+1} < F_{\ell+2}$ , then

$$\mathbf{M} = \begin{bmatrix} \mathbf{I}_{(F_{\ell+1}-1) \times (F_{\ell+1}-1)} & \mathbf{0}_{F_{\ell+1}} & \mathbf{0}_{(F_{\ell+1}-1) \times (F_{\ell+2}-F_{\ell+1})} \\ \mathbf{0}_{F_{\ell+1}-1} & 1 & \mathbf{1}_{F_{\ell+2}-F_{\ell+1}}^\top \end{bmatrix}.$$

If  $F_{\ell+1} > F_{\ell+2}$ , then

$$\mathbf{M} = \begin{bmatrix} \mathbf{I}_{(F_{\ell+1}-F_{\ell+2}) \times F_{\ell+2}} \\ \mathbf{0}_{F_{\ell+2} \times F_{\ell+2}} \end{bmatrix}.$$

If  $\ell = L_\phi$ , then all of the output channels may be computed with one matrix multiplication by

$$\begin{aligned} & [\mathbf{H}_{i,\ell}[1], \dots, \mathbf{H}_{i,\ell}[C_\ell], \mathbf{1}_{F_{\ell+1}}^\top] \begin{bmatrix} \mathbf{W}(1,1) & \dots & \mathbf{W}(1,C_{\ell+1}) \\ \vdots & \ddots & \vdots \\ \mathbf{W}(C_\ell,1) & \dots & \mathbf{W}(C_\ell,C_{\ell+1}) \\ w_{\text{bias}}(1)\mathbf{I} & \dots & w_{\text{bias}}(C_{\ell+1})\mathbf{I} \end{bmatrix} \\ &= [\text{Conv1d}_\ell(\mathbf{H}_{i,\ell})[1], \dots, \text{Conv1d}_\ell(\mathbf{H}_{i,\ell})[C_{\ell+1}]] \end{aligned}$$

**Lemma 9 (EqConv $_\ell$  as a linear layer)** *Assume that all input channels to EqConv $_\ell$  :  $\mathbb{R}^{C_\ell \times F_\ell} \rightarrow \mathbb{R}^{C_{\ell+1} \times F_{\ell+1}}$  are of length  $F_\ell$ , then EqConv $_\ell$  is expressible as a matrix multiplication with a fixed-dimension weight matrix.*

*Proof* EqConv $_\ell$  :  $\mathbb{R}^{C_\ell \times F_\ell} \rightarrow \mathbb{R}^{C_{\ell+1} \times F_{\ell+1}}$  has  $C_\ell/2$  input channels that are two-row matrices of the form

$$\mathbf{H}_{i,\ell}[c_{\text{in}}] = [\mathbf{g}_{c_{\text{in}},1}, \dots, \mathbf{g}_{c_{\text{in}},F_\ell}] \quad .$$

Arranging each input channel matrix end to end, an output channel  $c_{\text{out}} \in \{1, \dots, C_{\ell+1}/2\}$  is

$$\mathbf{H}_{i,\ell+1}[c_{\text{out}}] = \text{EqConv}_{\ell}(\mathbf{H}_{i,\ell})[c_{\text{out}}] = [\mathbf{H}_{i,\ell}[1], \dots, \mathbf{H}_{i,\ell}[C_{\ell}/2]] \begin{bmatrix} \mathbf{W}(1, c_{\text{out}}) \\ \vdots \\ \mathbf{W}(C_{\ell}/2, c_{\text{out}}) \end{bmatrix}.$$

All of the output channels may be computed with one matrix multiplication by

$$\begin{aligned} & [\mathbf{H}_{i,\ell}[1], \dots, \mathbf{H}_{i,\ell}[C_{\ell}/2]] \begin{bmatrix} \mathbf{W}(1, 1) & \dots & \mathbf{W}(1, C_{\ell+1}/2) \\ \vdots & \ddots & \vdots \\ \mathbf{W}(C_{\ell}/2, 1) & \dots & \mathbf{W}(C_{\ell}/2, C_{\ell+1}/2) \end{bmatrix} \\ &= [\text{EqConv}_{\ell}(\mathbf{H}_{i,\ell})[1], \dots, \text{EqConv}_{\ell}(\mathbf{H}_{i,\ell})[C_{\ell+1}/2]]. \end{aligned}$$

### A.2.2 Equivariant functions

**Lemma 10**  $O(n)$  equivariant functions  $\mathbf{F}$  satisfy  $\mathbf{F}(\mathbf{0}) = \mathbf{0}$ .

*Proof* By Proposition 1 in [21], there exists a function  $\tilde{\sigma}$  such that

$$\mathbf{F}(\mathbf{G}) = \mathbf{G}\tilde{\sigma}(\mathbf{G}^{\top}\mathbf{G}),$$

where the output of  $\tilde{\sigma}$  has the appropriate shape. Then,  $\mathbf{F}(\mathbf{0}) = \mathbf{0}\tilde{\sigma}(\mathbf{0}^{\top}\mathbf{0}) = \mathbf{0}$ .

### A.2.3 Lipschitz $O(n)$ equivariant functions

We derive a sufficient condition for an  $O(n)$  equivariant function to be Lipschitz.

**Lemma 11** Let  $\mathbf{f} : \mathbb{R}^n \rightarrow \mathbb{R}^n$  be an  $O(n)$  equivariant function. By Proposition 1 in [21],  $\mathbf{f}(\mathbf{x}) = \mathbf{x}\tilde{\sigma}(\|\mathbf{x}\|)$  where  $\tilde{\sigma}$  is scalar-valued. If  $\tilde{\sigma}$  is continuously differentiable,  $\lim_{x \rightarrow \infty} \tilde{\sigma}(x) < \infty$ , and  $\lim_{x \rightarrow \infty} x\tilde{\sigma}'(x) < \infty$ , then  $\mathbf{f}(\mathbf{x})$  is Lipschitz. Moreover,  $\mathbf{f}(\mathbf{x})$  has Lipschitz constant  $L = \max_{x \geq 0} \tilde{\sigma}(x) + x\tilde{\sigma}'(x)$ .

*Proof* We start by bounding the derivative of  $\mathbf{f}(\mathbf{x})$  in the spectral norm:

$$\begin{aligned} \left\| \frac{d}{d\mathbf{x}} \mathbf{f}(\mathbf{x}) \right\|_2 &= \left\| \tilde{\sigma}(\|\mathbf{x}\|)\mathbf{I} + \mathbf{x} \frac{d}{d\mathbf{x}} \tilde{\sigma}(\|\mathbf{x}\|) \right\|_2 \\ &= \left\| \tilde{\sigma}(\|\mathbf{x}\|)\mathbf{I} + \frac{\tilde{\sigma}'(\|\mathbf{x}\|)}{\|\mathbf{x}\|} \mathbf{x}\mathbf{x}^{\top} \right\|_2 \\ &\leq \|\tilde{\sigma}(\|\mathbf{x}\|)\mathbf{I}\|_2 + \left\| \frac{\tilde{\sigma}'(\|\mathbf{x}\|)}{\|\mathbf{x}\|} \mathbf{x}\mathbf{x}^{\top} \right\|_2 \\ &\leq \tilde{\sigma}(\|\mathbf{x}\|) + \frac{\tilde{\sigma}'(\|\mathbf{x}\|)}{\|\mathbf{x}\|} \|\mathbf{x}\|^2 \\ &= \tilde{\sigma}(\|\mathbf{x}\|) + \|\mathbf{x}\|\tilde{\sigma}'(\|\mathbf{x}\|) \end{aligned}$$

By the assumptions on  $\tilde{\sigma}$ ,

$$\left\| \frac{d}{d\mathbf{x}} \mathbf{f}(\mathbf{x}) \right\|_2 \leq \tilde{\sigma}(\|\mathbf{x}\|) + \|\mathbf{x}\|\tilde{\sigma}'(\|\mathbf{x}\|) < \infty.$$

Since  $\tilde{\sigma}$  is continuously differentiable,  $L = \sup_{x \geq 0} \tilde{\sigma}(x) + x\tilde{\sigma}'(x) < \infty$ . Finally,  $\mathbf{f}(\mathbf{x})$  is Lipschitz with constant  $L$  since, for  $\mathbf{a}, \mathbf{b} \in \mathbb{R}^n$ ,

$$\|\mathbf{f}(\mathbf{a}) - \mathbf{f}(\mathbf{b})\| \leq \|\mathbf{a} - \mathbf{b}\| \sup_{\mathbf{x}} \left\| \frac{d\mathbf{f}}{d\mathbf{x}}(\mathbf{x}) \right\|_2 \leq L\|\mathbf{a} - \mathbf{b}\|.$$

Next, we show that the block-wise application of a Lipschitz  $O(n)$  equivariant function is Lipschitz.

**Lemma 12** Let  $\mathbf{F} : \mathbb{R}^{n \times F_{\ell+1}} \rightarrow \mathbb{R}^{n \times F_{\ell+1}}$  be given by

$$\mathbf{F}(\mathbf{G}) = \mathbf{G} \odot \mathbf{1}_n[\tilde{\sigma}(\|\mathbf{g}_1\|), \dots, \tilde{\sigma}(\|\mathbf{g}_{F_{\ell+1}}\|)],$$

where  $\mathbf{f}(\mathbf{x}) = \mathbf{x}\tilde{\sigma}(\|\mathbf{x}\|)$  is  $O(2)$  equivariant and Lipschitz with constant  $L$ .  $\mathbf{F}(\mathbf{G})$  is Lipschitz with constant  $L$ :

$$\|\mathbf{F}(\mathbf{A}) - \mathbf{F}(\mathbf{B})\|_F \leq L\|\mathbf{A} - \mathbf{B}\|_F.$$

*Proof* This is proven using the definition of the Frobenius norm:

$$\|\mathbf{F}(\mathbf{A}) - \mathbf{F}(\mathbf{B})\|_F^2 = \sum_{f=1}^{F_{\ell+1}} \|\mathbf{f}(\mathbf{a}_f) - \mathbf{f}(\mathbf{b}_f)\|^2 \leq L^2 \sum_{f=1}^{F_{\ell+1}} \|\mathbf{a}_f - \mathbf{b}_f\|^2 \leq L^2 \|\mathbf{A} - \mathbf{B}\|_F^2,$$

Taking the square root of both sizes gives the result.

**Lemma 13** Let  $\mathbf{F} : \mathbb{R}^{(nC_{\ell+1}/n) \times F_{\ell+1}}$  such that  $C_{\ell+1}/n \in \mathbb{N}$ . For  $c_{\text{out}} \in \{1, \dots, C_{\ell+1}/n\}$  and  $\mathbf{G}$  where  $\mathbf{G}[c_{\text{out}}] = [\mathbf{g}_{c_{\text{out}},1}, \dots, \mathbf{g}_{c_{\text{out}},F_{\ell+1}}] \in \mathbb{R}^{n \times F_{\ell+1}}$ , suppose

$$\mathbf{F}(\mathbf{G})[c_{\text{out}}] = \mathbf{G}[c_{\text{out}}] \odot \mathbf{1}_n[\tilde{\sigma}(\|\mathbf{g}_{c_{\text{out}},1}\|), \dots, \tilde{\sigma}(\|\mathbf{g}_{c_{\text{out}},F_{\ell+1}}\|)].$$

If  $\mathbf{f} : \mathbb{R}^n \rightarrow \mathbb{R}^n$  is as defined in Lemma 12 with Lipschitz constant  $L$ , then

$$\|\mathbf{F}(\mathbf{A}) - \mathbf{F}(\mathbf{B})\|_F \leq L\|\mathbf{A} - \mathbf{B}\|_F.$$

*Proof* By Lemma 12 and the definition of the Frobenius norm,

$$\begin{aligned} \|\mathbf{F}(\mathbf{A}) - \mathbf{F}(\mathbf{B})\|_F^2 &= \sum_{c_{\text{out}}=1}^{C_{\ell+1}/n} \|\mathbf{F}(\mathbf{A})[c_{\text{out}}] - \mathbf{F}(\mathbf{B})[c_{\text{out}}]\|_F^2 \\ &\leq L^2 \sum_{c_{\text{out}}=1}^{C_{\ell+1}/n} \|\mathbf{A}[c_{\text{out}}] - \mathbf{B}[c_{\text{out}}]\|_F^2 = L^2 \|\mathbf{A} - \mathbf{B}\|_F^2. \end{aligned}$$

Taking the square root of both sizes gives the result.

Using Lemmas 11, 12, and 13, we show that the activations  $\sigma_{\ln}$  and  $\sigma_{\tanh}$  in  $\phi_{\text{EqConv}}$  are Lipschitz.

**Lemma 14**  $O(n)$  equivariant activation  $\sigma_{\ln}$  is Lipschitz.

*Proof* Define

$$\tilde{\sigma}_{\ln}(x) = \begin{cases} 1 & x = 0 \\ \frac{\ln(1+x)}{x} & x \neq 0 \end{cases}$$

with derivative

$$\tilde{\sigma}'_{\ln}(x) = \begin{cases} 0 & x = 0 \\ \frac{1}{x(1+x)} - \frac{\ln(1+x)}{x^2} & x \neq 0 \end{cases}.$$

In order to apply Lemma 11, we compute the following limits:

$$\begin{aligned} \lim_{x \rightarrow \infty} \tilde{\sigma}_{\ln}(x) &= \lim_{x \rightarrow \infty} \frac{\ln(1+x)}{x} \stackrel{\text{L'Hôpital}}{=} \lim_{x \rightarrow \infty} \frac{1}{1+x} = 0 < \infty, \\ \lim_{x \rightarrow \infty} x \tilde{\sigma}'_{\ln}(x) &= \lim_{x \rightarrow \infty} \frac{1}{1+x} - \frac{\ln(1+x)}{x} \\ &= 0 - \lim_{x \rightarrow \infty} \frac{\ln(1+x)}{x} \stackrel{\text{L'Hôpital}}{=} 0 - \lim_{x \rightarrow \infty} \frac{1}{1+x} = 0 - 0 = 0. \end{aligned}$$

By Lemma 11,  $\mathbf{f}(\mathbf{x}) = \mathbf{x}\tilde{\sigma}_{\ln}(\|\mathbf{x}\|)$  is Lipschitz with constant  $L = \max_{x \geq 0} \tilde{\sigma}_{\ln}(x) + x \tilde{\sigma}'_{\ln}(x)$ . Applying Lemmas 12 and 13,  $\sigma_{\ln}(\mathbf{G})$  is Lipschitz with constant  $L$ .

**Lemma 15**  $O(n)$  equivariant activation  $\sigma_{\tanh}$  is Lipschitz.

*Proof* Define  $\tilde{\sigma}_{\tanh}(x) = \tanh(x)$ , and then  $\tilde{\sigma}'_{\tanh}(x) = 1 - \tanh^2(x)$ . In order to apply Lemma 11, we compute the following limits:

$$\lim_{x \rightarrow \infty} \tilde{\sigma}_{\tanh}(x) = \lim_{x \rightarrow \infty} \tanh(x) = 1 < \infty,$$

$$\lim_{x \rightarrow \infty} x \tilde{\sigma}'_{\tanh}(x) = \lim_{x \rightarrow \infty} x(1 - \tanh^2(x)) \stackrel{\text{L'Hôpital}}{=} \lim_{x \rightarrow \infty} \frac{1}{\frac{2 \tanh(x)}{1 - \tanh^2(x)}} = \lim_{x \rightarrow \infty} \frac{1 - \tanh^2(x)}{2 \tanh(x)} = 0.$$

By Lemma 11,  $f(x) = x \tilde{\sigma}_{\tanh}(\|x\|)$  is Lipschitz with constant  $L = \max_{x \geq 0} \tilde{\sigma}_{\tanh}(x) + x \tilde{\sigma}'_{\tanh}(x)$ . Applying Lemmas 12 and 13,  $\sigma_{\tanh}(\mathbf{G})$  is Lipschitz with constant  $L$ .

### A.3 Obstacle avoidance

**Lemma 16**  $\gamma(\mathbf{r}, \mathbf{v}, \theta)$  from Eqn. (10) is invariant with respect to  $SO(2)$ .

*Proof* Let  $\mathbf{R} \in SO(2)$ .

$$\begin{aligned} \gamma(\mathbf{R}\mathbf{r}, \mathbf{R}\mathbf{v}, \theta) &= \frac{(\mathbf{R}\mathbf{r})^\top}{\|\mathbf{R}\mathbf{r}\|} \mathbf{R}(\theta) \frac{\mathbf{R}\mathbf{v}}{\|\mathbf{R}\mathbf{v}\|} = \frac{\mathbf{r}^\top \mathbf{R}^\top \mathbf{R}(\theta) \mathbf{R}\mathbf{v}}{\|\mathbf{r}\| \|\mathbf{v}\|} \\ &= \frac{\mathbf{r}^\top \mathbf{R}^\top \mathbf{R} \mathbf{R}(\theta) \mathbf{v}}{\|\mathbf{r}\| \|\mathbf{v}\|} \quad \text{since matrices of } SO(2) \text{ commute} \\ &= \frac{\mathbf{r}^\top \mathbf{I} \mathbf{R}(\theta) \mathbf{v}}{\|\mathbf{r}\| \|\mathbf{v}\|} = \gamma(\mathbf{r}, \mathbf{v}, \theta). \end{aligned}$$

Therefore,  $\gamma$  is invariant with respect to  $SO(2)$ .

**Proposition 3** The relative velocity in Eqn. (11) is equivariant with respect to  $SO(2)$ .

*Proof* Let  $\mathbf{R} \in SO(2)$ . First,  $\bar{\mathbf{v}}_i$  is equivariant with respect to  $SO(2)$  since

$$\text{mean}\{\mathbf{R}\dot{\mathbf{x}}_j(t) : j \in \mathcal{N}_i(t)\} = \mathbf{R} \text{mean}\{\dot{\mathbf{x}}_j(t) : j \in \mathcal{N}_i(t)\} = \mathbf{R}\bar{\mathbf{v}}_i(t).$$

We check each case of the relative velocity formula. When  $-\alpha_2 \leq \gamma(\mathbf{r}_{ji}, \bar{\mathbf{v}}_i, 0) \leq 0$ ,

$$\begin{aligned} \alpha_1(\|\mathbf{R}\mathbf{r}_{ji}\|, \|\mathbf{R}\bar{\mathbf{v}}_i\|) \frac{\mathbf{R}\mathbf{r}_{ji}}{\|\mathbf{R}\mathbf{r}_{ji}\|} &= \alpha_1(\|\mathbf{r}_{ji}\|, \|\bar{\mathbf{v}}_i\|) \frac{\mathbf{R}\mathbf{r}_{ji}}{\|\mathbf{r}_{ji}\|} \\ &= \mathbf{R} \alpha_1(\|\mathbf{r}_{ji}\|, \|\bar{\mathbf{v}}_i\|) \frac{\mathbf{r}_{ji}}{\|\mathbf{r}_{ji}\|} = \mathbf{R}(-\dot{\mathbf{r}}_{ij}(t)). \end{aligned}$$

For the other case,

$$\begin{aligned} &\alpha_1(\|\mathbf{R}\mathbf{r}_{ji}\|, \|\mathbf{R}\bar{\mathbf{v}}_i\|) (-\text{sgn}[\gamma(\mathbf{R}\mathbf{r}_{ji}, \mathbf{R}\bar{\mathbf{v}}_i, \frac{\pi}{2})] \mathbf{R}(\alpha_\theta)) \frac{\mathbf{R}\mathbf{r}_{ji}}{\|\mathbf{R}\mathbf{r}_{ji}\|} \\ &= \alpha_1(\|\mathbf{r}_{ji}\|, \|\bar{\mathbf{v}}_i\|) (-\text{sgn}[\gamma(\mathbf{r}_{ji}, \bar{\mathbf{v}}_i, \frac{\pi}{2})] \mathbf{R}(\alpha_\theta)) \frac{\mathbf{R}\mathbf{r}_{ji}}{\|\mathbf{r}_{ji}\|} \\ &= \mathbf{R} \alpha_1(\|\mathbf{r}_{ji}\|, \|\bar{\mathbf{v}}_i\|) (-\text{sgn}[\gamma(\mathbf{r}_{ji}, \bar{\mathbf{v}}_i, \frac{\pi}{2})] \mathbf{R}(\alpha_\theta)) \frac{\mathbf{r}_{ji}}{\|\mathbf{r}_{ji}\|} \quad \text{since matrices of } SO(2) \text{ commute} \\ &= \mathbf{R}(-\dot{\mathbf{r}}_{ij}(t)). \end{aligned}$$

Therefore, the relative velocity is  $SO(2)$  equivariant.

## References

1. Akyildiz, I.F., Su, W., Sankarasubramaniam, Y., Cayirci, E.: A survey on sensor networks. *IEEE Communications magazine* **40**(8), 102–114 (2002). DOI <https://doi.org/10.1109/MCOM.2002.1024422>
2. Baker, J., Wang, S.H., de Fernex, T., Wang, B.: An explicit frame construction for normalizing 3d point clouds. In: *Forty-first International Conference on Machine Learning* (2024). URL <https://openreview.net/forum?id=SZ0JnRxi0x>
3. Bartlett, P.L., Foster, D.J., Telgarsky, M.J.: Spectrally-normalized margin bounds for neural networks. In: I. Guyon, U.V. Luxburg, S. Bengio, H. Wallach, R. Fergus, S. Vishwanathan, R. Garnett (eds.) *Advances in Neural Information Processing Systems*, vol. 30. Curran Associates, Inc. (2017). URL [https://proceedings.neurips.cc/paper\\_files/paper/2017/file/b22b257ad0519d4500539da3c8bcf4dd-Paper.pdf](https://proceedings.neurips.cc/paper_files/paper/2017/file/b22b257ad0519d4500539da3c8bcf4dd-Paper.pdf)
4. Brandstetter, J., Hesselink, R., van der Pol, E., Bekkers, E.J., Welling, M.: Geometric and physical quantities improve E(3) equivariant message passing. In: *International Conference on Learning Representations* (2022). URL [https://openreview.net/forum?id=\\_xwr8g0BeV1](https://openreview.net/forum?id=_xwr8g0BeV1)
5. Camazine, S. (ed.): *Self-Organization in Biological Systems*, 2. print., and 1. paperback print edn. Princeton Studies in Complexity. Princeton Univ. Press. DOI <https://doi.org/10.2307/j.ctvzxx9tx>
6. Chen, M., Li, X., Zhao, T.: On generalization bounds of a family of recurrent neural networks (2019). URL <https://openreview.net/forum?id=Skf-oo0qt7>
7. Choi, Y.P., Ha, S.Y., Li, Z.: *Emergent Dynamics of the Cucker–Smale Flocking Model and Its Variants*, pp. 299–331. Springer International Publishing, Cham (2017). DOI [https://doi.org/10.1007/978-3-319-49996-3\\_8](https://doi.org/10.1007/978-3-319-49996-3_8)
8. Choi, Y.P., Kalise, D., Peszek, J., Peters, A.A.: A collisionless singular cucker–smale model with decentralized formation control. *SIAM Journal on Applied Dynamical Systems* **18**(4), 1954–1981 (2019). DOI <https://doi.org/10.1137/19M1241799>
9. Choi, Y.P., Oh, D., Tse, O.: Controlled pattern formation of stochastic cucker–smale systems with network structures. *Communications in Nonlinear Science and Numerical Simulation* **111**, 106474 (2022). DOI <https://doi.org/10.1016/j.cnsns.2022.106474>
10. Cohen, T.S., Welling, M.: Steerable CNNs. In: *International Conference on Learning Representations* (2017). URL <https://openreview.net/forum?id=rJQKYt511>
11. Cucker, F., Dong, J.G.: Avoiding Collisions in Flocks **55**(5), 1238–1243. DOI <https://doi.org/10.1109/TAC.2010.2042355>. URL <http://ieeexplore.ieee.org/document/5406110/>
12. Cucker, F., Smale, S.: Emergent Behavior in Flocks **52**(5), 852–862. DOI <https://doi.org/10.1109/TAC.2007.895842>
13. Fuchs, F., Worrall, D., Fischer, V., Welling, M.: Se (3)-transformers: 3d roto-translation equivariant attention networks. *Advances in neural information processing systems* **33**, 1970–1981 (2020). URL <https://papers.neurips.cc/paper/2020/file/15231a7ce4ba789d13b722cc5c955834-Paper.pdf>
14. Garg, V., Jegelka, S., Jaakkola, T.: Generalization and representational limits of graph neural networks. In: *International Conference on Machine Learning*, pp. 3419–3430. PMLR (2020). URL <https://proceedings.mlr.press/v119/garg20c/garg20c.pdf>
15. Gu, D., Wang, Z.: Leader–Follower Flocking: Algorithms and Experiments **17**(5), 1211–1219. DOI <https://doi.org/10.1109/TCST.2008.2009461>. URL <http://ieeexplore.ieee.org/document/4895844/>
16. Hua, Y., Miller, K., Bertozzi, A.L., Qian, C., Wang, B.: Efficient and reliable overlay networks for decentralized federated learning. *SIAM Journal on Applied Mathematics* **82**(4), 1558–1586 (2022). DOI <https://doi.org/10.1137/21M1465081>
17. Hua, Y., Pang, J., Zhang, X., Liu, Y., Shi, X., Wang, B., Liu, Y., Qian, C.: Towards practical overlay networks for decentralized federated learning. *arXiv preprint arXiv:2409.05331* (2024). DOI <https://doi.org/10.48550/arXiv.2409.05331>
18. Karczewski, R., Souza, A.H., Garg, V.: On the generalization of equivariant graph neural networks. In: R. Salakhutdinov, Z. Kolter, K. Heller, A. Weller, N. Oliver, J. Scarlett, F. Berkenkamp (eds.) *Proceedings of the 41st International Conference on Machine Learning, Proceedings of Machine Learning Research*, vol. 235, pp. 23159–23186. PMLR. URL <https://proceedings.mlr.press/v235/karczewski24a.html>

19. Kondor, R., Trivedi, S.: On the generalization of equivariance and convolution in neural networks to the action of compact groups. In: J. Dy, A. Krause (eds.) *Proceedings of the 35th International Conference on Machine Learning, Proceedings of Machine Learning Research*, vol. 80, pp. 2747–2755. PMLR (2018). URL <https://proceedings.mlr.press/v80/kondor18a.html>
20. Lawrence, H., Georgiev, K., Dienes, A., Kiani, B.T.: Implicit bias of linear equivariant networks. In: K. Chaudhuri, S. Jegelka, L. Song, C. Szepesvari, G. Niu, S. Sabato (eds.) *Proceedings of the 39th International Conference on Machine Learning, Proceedings of Machine Learning Research*, vol. 162, pp. 12096–12125. PMLR (2022). URL <https://proceedings.mlr.press/v162/lawrence22a/lawrence22a.pdf>
21. Ma, C., Ying, L.: Why self attention is natural for sequence-to-sequence problems? a perspective from symmetries (2023). URL <https://openreview.net/forum?id=dNdOnKy9YNs>
22. Minakowski, P., Mucha, P.B., Peszek, J., Zatorska, E.: *Singular Cucker–Smale Dynamics*, pp. 201–243. Springer International Publishing, Cham (2019). DOI [https://doi.org/10.1007/978-3-030-20297-2\\_7](https://doi.org/10.1007/978-3-030-20297-2_7)
23. Mohri, M., Rostamizadeh, A., Talwalkar, A.: *Foundations of Machine Learning. Adaptive Computation and Machine Learning*. The MIT Press. URL <https://mitpress.mit.edu/9780262039406/foundations-of-machine-learning/>
24. Oh, D.: Flocking Behavior in Stochastic Cucker-Smale Model with Formation Control on Symmetric Digraphs. URL <http://www.riss.kr/link?id=T15771814>
25. Omotuyi, O., Kumar, M.: Learning Decentralized Controllers for Segregation of Heterogeneous Robot Swarms with Graph Neural Networks. In: *2022 International Conference on Manipulation, Automation and Robotics at Small Scales (MARSS)*, pp. 1–6. IEEE. DOI <https://doi.org/10.1109/MARSS55884.2022.9870482>
26. Park, J., Kim, H.J., Ha, S.Y.: Cucker-Smale Flocking With Inter-Particle Bonding Forces **55**(11), 2617–2623. DOI <https://doi.org/10.1109/TAC.2010.2061070>
27. Parrish, J.K., Viscido, S.V., Grünbaum, D.: Self-Organized Fish Schools: An Examination of Emergent Properties **202**(3), 296–305. DOI <https://doi.org/10.2307/1543482>. URL <https://www.journals.uchicago.edu/doi/10.2307/1543482>
28. Perea, L., Gómez, G., Elosegui, P.: Extension of the cucker-smale control law to space flight formations. *Journal of guidance, control, and dynamics* **32**(2), 527–537 (2009). DOI <https://doi.org/10.2514/1.36269>
29. van der Pol, E., Worrall, D., van Hoof, H., Oliehoek, F., Welling, M.: MDP homomorphic networks: Group symmetries in reinforcement learning. *Advances in Neural Information Processing Systems* **33**, 4199–4210 (2020). URL <https://proceedings.neurips.cc/paper/2020/file/2be5f9c2e3620eb73c2972d7552b6cb5-Paper.pdf>
30. Reynolds, C.W.: Flocks, herds and schools: A distributed behavioral model **21**(4), 25–34. DOI <https://doi.org/10.1145/37402.37406>. URL <https://dl.acm.org/doi/10.1145/37402.37406>
31. Ross, S., Gordon, G., Bagnell, D.: A reduction of imitation learning and structured prediction to no-regret online learning. In: G. Gordon, D. Dunson, M. Dudík (eds.) *Proceedings of the Fourteenth International Conference on Artificial Intelligence and Statistics, Proceedings of Machine Learning Research*, vol. 15, pp. 627–635. PMLR, Fort Lauderdale, FL, USA (2011). URL <https://proceedings.mlr.press/v15/ross11a.html>
32. Santos, V.G., Pimenta, L.C.A., Chaimowicz, L.: Segregation of multiple heterogeneous units in a robotic swarm. In: *2014 IEEE International Conference on Robotics and Automation (ICRA)*, pp. 1112–1117. IEEE. DOI <https://doi.org/10.1109/ICRA.2014.6906993>
33. Satorras, V.G., Hoogeboom, E., Welling, M.: E(n) equivariant graph neural networks. In: *International conference on machine learning*, pp. 9323–9332. PMLR (2021). URL <https://proceedings.mlr.press/v139/satorras21a/satorras21a.pdf>
34. Sun, T., Li, D., Wang, B.: Decentralized federated averaging. *IEEE Transactions on Pattern Analysis and Machine Intelligence* **45**(4), 4289–4301 (2023). DOI <https://doi.org/10.1109/TPAMI.2022.3196503>
35. Tanner, H., Jadbabaie, A., Pappas, G.: Stable flocking of mobile agents. I. Fixed topology. In: *42nd IEEE International Conference on Decision and Control (IEEE Cat. No.03CH37475)*, vol. 2, pp. 2010–2015. IEEE. DOI <https://doi.org/10.1109/CDC.2003.1272910>



36. Tanner, H., Jadbabaie, A., Pappas, G.: Stable flocking of mobile agents. II. Dynamic topology. In: 42nd IEEE International Conference on Decision and Control (IEEE Cat. No.03CH37475), vol. 2, pp. 2016–2021. IEEE. DOI <https://doi.org/10.1109/CDC.2003.1272911>
37. Tolstaya, E., Gama, F., Paulos, J., Pappas, G., Kumar, V., Ribeiro, A.: Learning decentralized controllers for robot swarms with graph neural networks. In: Conference on robot learning, pp. 671–682. PMLR (2020). URL <https://proceedings.mlr.press/v100/tolstaya20a.html>
38. Wang, S.H., Hsu, Y.C., Baker, J., Bertozzi, A.L., Xin, J., Wang, B.: Rethinking the benefits of steerable features in 3d equivariant graph neural networks. In: The Twelfth International Conference on Learning Representations (2024). URL <https://openreview.net/forum?id=mGHJAYR8wO>
39. Weiler, M., Cesa, G.: General  $e(2)$ -equivariant steerable cnns. *Advances in neural information processing systems* **32** (2019). URL [https://proceedings.neurips.cc/paper\\_files/paper/2019/file/45d6637b718d0f24a237069fe41b0db4-Paper.pdf](https://proceedings.neurips.cc/paper_files/paper/2019/file/45d6637b718d0f24a237069fe41b0db4-Paper.pdf)
40. Weimerskirch, H., Martin, J., Clerquin, Y., Alexandre, P., Jiraskova, S.: Energy saving in flight formation **413**(6857), 697–698. DOI <https://doi.org/10.1038/35099670>. URL <https://www.nature.com/articles/35099670>
41. Yarotsky, D.: Universal approximations of invariant maps by neural networks. *Constructive Approximation* **55**(1), 407–474 (2022). DOI <https://doi.org/10.1007/s00365-021-09546-1>